

CHEMICAL COMPOSITIONS OF RED GIANT STARS IN OLD LARGE MAGELLANIC CLOUD GLOBULAR CLUSTERS

JENNIFER A. JOHNSON¹

Dominion Astrophysical Observatory, Herzberg Institute of Astrophysics, National Research Council, 5071 West Saanich Rd., Victoria,
BC V9E 2E7, Canada and
Observatories of the Carnegie Institute of Washington, Pasadena, CA 91101 USA

INESE I. IVANS^{2,3,4}

Department of Astronomy, California Institute of Technology, Pasadena, CA 91125 USA

AND

PETER B. STETSON

Dominion Astrophysical Observatory, Herzberg Institute of Astrophysics, National Research Council, 5071 West Saanich Rd., Victoria,
BC V9E 2E7, Canada

Draft version October 29, 2018

ABSTRACT

We have observed ten red giant stars in four old Large Magellanic Cloud globular clusters with the high-resolution spectrograph MIKE on the Magellan Landon Clay 6.5-m telescope. The stars in our sample have up to 20 elemental abundance determinations for the α -, iron-peak, and neutron-capture element groups. We have also derived abundances for the light odd-Z elements Na and Al. We find NGC 2005 and NGC 2019 to be more metal-rich than previous estimates from the Ca II triplet, and we derive [Fe/H] values closer to those obtained from the slope of the red giant branch. However, we confirm previous determinations for Hodge 11 and NGC 1898 to within 0.2 dex. The LMC cluster [Mg/Fe] and [Si/Fe] ratios are comparable to the values observed in old Galactic globular cluster stars, as are the abundances [Y/Fe], [Ba/Fe], and [Eu/Fe]. The LMC clusters do not share the low-Y behavior observed in some dwarf spheroidal galaxies. [Ca/Fe], [Ti/Fe], and [V/Fe] in the LMC, however, are *significantly* lower than what is seen in the Galactic globular cluster system. Neither does the behavior of [Cu/Fe] as a function of [Fe/H] in our LMC clusters match the trend seen in the Galaxy, staying instead at a constant value of ~ -0.8 . Because not all $[\alpha/\text{Fe}]$ ratios are suppressed, these abundance ratios cannot be attributed solely to the injection of Type Ia SNe material, and instead reflect the differences in star formation history of the LMC vs. the Milky Way. An extensive numerical experimental study was performed, varying both input parameters and stellar atmosphere models, to verify that the unusual abundance ratios derived in this study are not the result of the adopted atomic parameters, stellar atmospheres or stellar parameters. We conclude that many of the abundances in the LMC globular clusters we observed are distinct from those observed in the Milky Way, and these differences are intrinsic to the stars in those systems.

Subject headings: nuclear reactions, nucleosynthesis, abundances – Magellanic Clouds – globular clusters:general – globular clusters:individual (Hodge 11, NGC 1898, NGC 2019, NGC 2005) – stars:abundances – stars:Population II – stars:fundamental parameters

1. INTRODUCTION

Globular clusters have been key to gaining insights into the early epoch of formation and evolution for galaxies in general and for the Galaxy in particular. Because of the proximity of Galactic globular clusters (GGC) to us, we can obtain color-magnitude diagrams and high-resolution spectra of individual stars, which has allowed us to measure ages and abundances with unique accuracy. These data show a complex and interesting pic-

ture for the GGC, including a dispersion in abundance ratios, trends in ratios with kinematics, and the possibility of the capture of clusters from other galaxies. We can now observe clusters in other galaxies of the Local Group with the same techniques to compare their cluster systems with the GGC and determine the variation in globular cluster systems from galaxy to galaxy and the possible contributions of other galaxies to the Milky Way system.

The Magellanic Clouds, less distant than some GGCs, provide an excellent opportunity to observe abundance patterns in another globular cluster system in detail. The Large Magellanic Cloud (LMC) has long been known to harbour clusters of similar age, mass and metallicity to the GGCs (Searle, Wilkinson, & Bagnuolo 1980). Testa et al. (1995) and Brocato et al. (1996) provided the first ages based on main-sequence turnoff measurements of the oldest clusters in the LMC. The main-sequence turnoffs in a large number of old clusters in the LMC

¹ Present Address: Department of Astronomy, Ohio State University, 140 West 18th Avenue, Columbus, OH 43210
Electronic address: Jennifer.Johnson@nrc-cnrc.gc.ca

² Hubble Fellow

³ Present Address: The Observatories of the the Carnegie Institution of Washington, Pasadena, CA 91101

⁴ Present Address: Princeton University Observatory, Peyton Hall, Princeton, NJ 08544
Electronic address: iii@ociw.edu
Electronic address: Peter.Stetson@nrc-cnrc.gc.ca

have subsequently been observed with the Hubble Space Telescope (HST). Some clusters in the LMC are coeval with nearby GGCs, such as M5, M4, and M92 (Olsen et al. 1998, LMC-O98, hereafter; Johnson et al. 1999, LMC-J99, hereafter).

The ages, kinematics, metallicities and abundance ratios of the GGCs have provided much insight into the formation of the Galaxy. Searle & Zinn (1978) argued that the outer halo clusters were younger than the inner halo clusters and that implied that a slow, chaotic buildup of the outer parts of the Galaxy had occurred. That mergers have contributed to the formation of the Galaxy was clearly shown with the discovery that the Sagittarius dwarf spheroidal galaxy (dSph) is currently being subsumed by the Milky Way (Ibata et al. 1994). The positions of GGCs on great circle orbits (Buonanno et al. 1994) that sometimes include other satellites of the Milky Way (Fusi Pecci et al. 1995) hint at past accretion events. Lin & Richer (1992) argued that the positions and radial velocities of Rup 106 and possibly Pal 12 suggest that they had been tidally captured from the Magellanic Clouds (MC). By incorporating proper motions in the analysis, Dinescu et al. (2000) suggested that it was more likely that Sagittarius was the original host galaxy of Pal 12. Bellazzini, Ferraro, & Ibata (2003) extended the analysis to conclude that at least four outer halo GGCs belonged to Sagittarius, in addition to the four clusters whose positions lie near the main body of Sagittarius (Ibata et al. 1995)

Information about the history of the Galaxy is also contained in the chemical abundance ratios of old stars. In a seminal paper, Tinsley (1979) argued that enhanced $[\alpha/\text{Fe}]$ -ratios⁵ in metal-poor stars were a consequence of the different timescales for the production of the α -elements (e.g., O, Ne, Mg, Si, Ca, and sometimes Ti) in core-collapse supernovae (Type II SNe) vs. the Fe produced by both SNe Type Ia and Type II. SNe Type II progenitors are short-lived (1Myr–100Myr) massive stars whereas progenitors of SNe Type Ia (mass-exchange binary systems including a white dwarf star) require longer to evolve and do not contribute to the chemical evolution of the Galaxy until $\geq 1\text{Gyr}$ subsequent to the formation of the binary system (Timmer, Woosley, & Weaver 1995; Matteucci & Recchi 2001). Hence, the ratio of Type Ia/Type II SNe events determines the $[\alpha/\text{Fe}]$. Systems that have recently started forming stars and have only had the contributions from massive stars to the interstellar medium would then be predicted to possess low Type Ia/II ratios and $[\alpha/\text{Fe}] > 0$. Old GGCs possess high $[\alpha/\text{Fe}]$ ratios (Pilachowski, Sneden, & Wallerstein 1983; and references therein), in accord with the idea that GGCs were among the first surviving Galactic objects to have formed.

Nissen & Schuster (1997; hereafter, NS97) discovered a sample of moderately metal-poor field stars with low $[\alpha/\text{Fe}]$ ratios and suggested that they could have accreted from dwarf galaxies with a chemical evolution history different than that of the solar neighborhood, allowing the material out of which they formed to include the ejecta

⁵ We adopt the usual spectroscopic notation that $[A/B] \equiv \log_{10}(N_A/N_B)_* - \log_{10}(N_A/N_B)_\odot$, and $\log \epsilon(A) \equiv \log_{10}(N_A/N_H) + 12.0$, for elements A and B. Also, in this paper, except for instances where $[m/H]$ or Z are specifically stated, we define metallicity as the stellar $[\text{Fe}/\text{H}]$.

from Type Ia SNe while they were still relatively metal-poor. Also exhibiting low $[\alpha/\text{Fe}]$ ratios with respect to the general GGC population are Rup 106 and Pal 12 (Brown, Wallerstein, & Zucker 1997), which are 2-3 Gyr younger than other GGCs (Buonanno et al. 1990; Stetson et al. 1989). Brown et al. interpreted the solar $[\alpha/\text{Fe}]$ -ratios to be the result of the cluster being formed long enough after star formation had begun in the surrounding region to have its abundance ratios substantially affected by contributions of iron from Type Ia SNe.

The characteristics of the production sites of other elements may also provide insight into timescales, initial mass functions, and other properties of clusters. At this time, both the predictions from theory and the data from globular clusters are murkier than the case of $[\alpha/\text{Fe}]$. For example, the site of the rapid neutron-capture process (*r*-process) is uncertain, but it is clear that the *r*-processed material appears before the slow-neutron-capture process (*s*-process) in asymptotic giant branch stars begins to contribute much to Galactic chemical evolution (Truran 1981). The *r*-process produces some heavy elements, such as Eu, more readily than others, such as Ba and La, while the *s*-process does the opposite. Therefore, ratios such as $[\text{Ba}/\text{Fe}]$ and $[\text{Ba}/\text{Eu}]$ contain information about when clusters formed from a chemical evolution standpoint. Other element ratios are also sensitive to the mix of stars that polluted the ISM. First, the metallicity of the progenitor of a Type II SNe is important in the synthesis of such elements as Na, Al, and Cu (e.g., Arnett 1971, Woosley & Weaver 1995). Second, the mass of the SN affects the ratio of the α elements produced (e.g. Woosley & Weaver 1995; McWilliam 1997). Less massive stars make lower ratios of $[\text{Mg}/\text{Ca}]$ and $[\text{Mg}/\text{Si}]$, for example. $[\text{Si}/\text{Ti}]$ should be highest for a 20 M_\odot star according to the Woosley & Weaver yields.

Recent efforts to measure many elements in globular clusters have shown that other abundance ratios, such as the ones listed above, vary between GGCs. Ivans et al. (1999; 2001; hereafter M4-I99 and M5-I01), measured abundance ratios of 14 elements in 36 giants in each of M4 and M5, two GGCs with similar $[\text{Fe}/\text{H}]$ and ages. Within either cluster, the stars possess comparable abundance ratios for elements not sensitive to proton-capture nucleosynthesis, but the same is not true of a comparison between clusters. Confirming and expanding upon the earlier results of Brown & Wallerstein (1992), M4-I99 found that the mean $[\text{Si}/\text{Fe}]$ ratio for the M4 stars is $3\text{-}\sigma$ greater than in M5 stars. The abundances of $[\text{Al}/\text{Fe}]$, $[\text{Ba}/\text{Fe}]$, and $[\text{La}/\text{Fe}]$ are also significantly higher in M4 stars. Interestingly, these clusters also differ in their apogalactic distances, with apogalactocentric radii of 5.9 and 35.4 kpc for M4 and M5, respectively (Dinescu et al. 1999). This same apparent trend with apogalactic distance and some abundance ratios may also be reflected in halo field and cluster stars (NS97; Hanson et al. 1998; Stephens 1999; Fulbright 2002; Lee & Carney 2002; Fulbright 2004). However, employing an extensive sample from the literature which included the results incorporated in Stephens (1999) and Fulbright (2004), Venn et al. (2004) argue that the low $[\alpha/\text{Fe}]$ ratios in halo stars are, if anything, correlated with extreme retrograde orbits and statistically not correlated with apogalactic distance.

Additional cluster-to-cluster abundance variations

have been found in other studies. Pursuing the investigation of the $[\alpha/\text{Fe}]$ trends to the inner halo, Lee & Carney (2002) report high $[\text{Si}/\text{Fe}]$ and low $[\text{Ti}/\text{Fe}]$ in NGC 6287, NGC6293, and NGC6541, three metal-poor GCC ($-1.8 \leq [\text{Fe}/\text{H}] \leq -2.0$). Lee, Carney, & Habgood (2004) report high $[\text{Si}/\text{Fe}]$ and low $[\text{Ti}/\text{Fe}]$ in M68 stars as well. Pal 12 stars, in addition to low $[\alpha/\text{Fe}]$ compared with other GGCs, also possess subsolar values of $[\text{Na}/\text{Fe}]$ and $[\text{Ni}/\text{Fe}]$ (Brown et al. 1997; Cohen 2004). Ter 7 stars show low $[\text{Ni}/\text{Fe}]$ (Tautvaišienė et al. 2004). As these examples illustrate, the evidence for abundance variations between GGCs has been firmly established

Within an individual GGC, star-to-star variations are observed among the light elements sensitive to proton-capture nucleosynthesis (e.g., C, N, O, Na, Mg, and Al). Early detections of CN variations among giant stars by Lindblad (1922) and Popper (1947) were expanded to higher resolution (see e.g., Osborn 1971; Peterson 1980) and, for some GGCs, to stars on the main sequence (see Hesser 1978; Hesser & Bell 1980). Also observed in globular cluster populations (but absent in the field star population) are anti-correlations in the abundances of $[\text{O}/\text{Fe}]$ with $[\text{Na}/\text{Fe}]$ and $[\text{Al}/\text{Fe}]$ (see Gratton, Sneden, & Carretta 2004 for a recent review).

One possible explanation for the light-element abundance patterns is “deep” mixing in red giants (e.g., Sweigart & Mengel 1979; Denissenkov & Weiss 1996, Denissenkov & Vandenberg 2003), dredging up the products of proton-capture nucleosynthesis from the interior out to the photosphere. It remains unclear, however, how the temperatures of the interiors of the red giant stars can even get hot enough to convert Mg to Al (Langer, Hoffman, & Zaidins 1997; Messenger & Lattanzio 2002). For some time, it had been thought that intermediate-mass asymptotic giant branch (AGB) stars could be responsible for producing the abundance patterns (Cottrell & Da Costa 1981), but recent work by Denissenkov & Herwig (2003) and Fenner et al. (2004) show that the observed abundance correlations are not replicated in model yields of AGB stars.

The presence of the abundance correlations at or below the main-sequence turnoff suggests that the variations may be primordial or the result of pollution by more evolved stars. It is likely that some combination of effects are at work. In M13, for example, the abundance patterns are also correlated with the evolutionary state of the stars (Kraft et al. 1993; Sneden et al. 2004; Johnson et al. 2005). While all clusters that have been examined for deep mixing effects show the associated abundance anomalies, some clusters appear to be more affected than others. The classic example is M3 and M13 (Kraft et al. 1992), where stars in M13 have $[\text{O}/\text{Fe}]$ down to values of -0.87 , while the most oxygen-poor stars M3 stars have $[\text{O}/\text{Fe}] = -0.25$. Other abundance ratios of light elements sensitive to proton-capture nucleosynthesis are similarly extreme in M13 but not in M3 (see e.g., Johnson et al. 2005 and references therein).

To summarize the situation in the GCC system, the majority of clusters exhibit super-solar $[\alpha/\text{Fe}]$ ratios, abundance ratio trends with apogalactic distance or prograde/retrograde orbits, solar iron-peak element ratios, and evidence of abundance correlations in the light elements, possibly due to deep mixing. *Are these universal properties of old globular cluster systems, or do they rep-*

resent the unique history of the Milky Way?

Low-dispersion spectra of individual giants by Cowley & Hartwick (1982) were used to measure spectral indices for nine old LMC clusters, including Hodge 11. Subsequently, Olszewski et al. (1991, LMC-O91) performed a comprehensive study to measure the metallicities of the LMC clusters using low-dispersion spectra of the Ca II infrared triplet lines in individual giants. These measurements have been extremely useful in tracing the age-metallicity relationship in the LMC and in providing estimates of the overall metallicity. However, for some Magellanic Cloud clusters (e.g., NGC 2019 and NGC 2005), there is a disagreement between the metallicities from LMC-O91 and the slopes of the red giant branches measured by LMC-O98. Abundance ratio questions could not be addressed, however, until high-resolution studies of LMC stars became available. The study by Hill et al. (2000) included LMC clusters of a range of ages, including one old cluster: NGC 2210 ($[\text{Fe}/\text{H}] = -1.75$). The three stars observed in NGC 2210 have $[\text{O}/\text{Fe}]$ values of 0.02, 0.19 and 0.21 dex, lower than are typical in GGC red giant stars. Smith et al. (2002) observed one star in NGC 1898 in the near-IR with PHOENIX on Gemini. $[\text{Ti}/\text{Fe}]$ is low in this star, illustrating that, for this cluster at least, LMC clusters do not always exhibit the high $[\alpha/\text{Fe}]$ abundances that typically belong to old GGCs.

In this paper, we report on abundances in four clusters in the Large Magellanic Cloud (LMC) observed with the MIKE spectrograph on Magellan. These clusters, NGC 1898, NGC 2005, NGC 2019 and Hodge 11 are globular clusters with ages from color-magnitude diagrams that are as old as the majority of GGCs (LMC-O98, LMC-J99) and have metallicities ranging from -2.0 to -1.0 . Therefore, they are similar to the kinds of GGC that have been important in deciphering the history of the Galactic spheroid.

2. OBSERVATIONS AND REDUCTIONS

2.1. Target Selection

To expand the sample of LMC cluster stars with high-resolution spectra and abundance ratio determinations for a large number of elements, we observed four old LMC clusters: Hodge 11, NGC 1898, NGC 2005, and NGC 2019. Hodge 11 is located 4.7° from the center. The other three clusters are located within 1.5° of the center of the LMC and are suitable comparisons to the inner halo GCCs.

LMC clusters are far enough away that stellar crowding leading to blended spectra is a potential problem, and this was one of the main concerns in the sample selection of LMC-O91. However, we cannot simply choose stars in the outskirts of the clusters, especially for clusters in the inner part of the LMC, since the ratio of field stars to cluster stars increases rapidly with radius. Instead, we employed the HST images obtained by LMC-O98 for NGC 1898, NGC 2005, and NGC 2019 to identify the brightest stars in the inner clusters whose stellar profiles are not apparently blended with the profiles of other bright stars. For Hodge 11, well removed from the LMC bar and disk, we chose the brightest uncrowded stars from a private catalog maintained by one of the authors (Stetson). Both Hodge 11 stars are saturated in the HST observations of LMC-J99. Only one of the stars is included in the observations of Mighell et al. (1996),

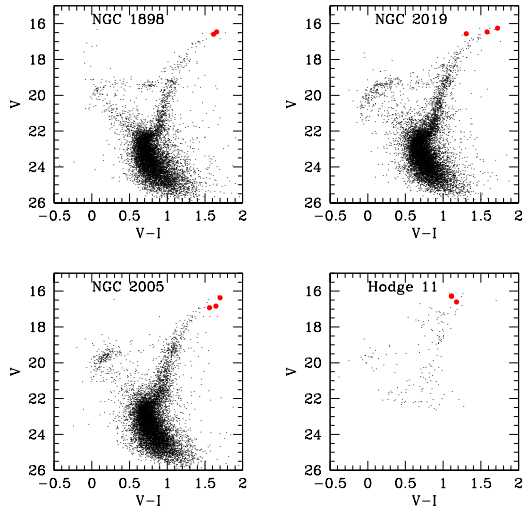


FIG. 1.— The color-magnitude diagrams for NGC 1898, NGC 2005, NGC 2019, and Hodge 11. The photometry is from LMC-O98 and a privately maintained catalog of one of the authors (Stetson). The stars we observed are indicated by large filled circles.

and it is saturated in the V exposures. As can be seen in Figure 1, all of our observed clusters stars lie at the tip of the giant branch.

2.2. Observations and Reductions

We observed the LMC globular cluster stars 27 December 2002 – 1 January 2003 with MIKE, the double echelle spectrograph (Bernstein et al. 2003) on the Magellan Landon Clay 6.5-m Telescope at the Las Campanas Observatory. The observations are summarized in Table 1, where we also list other names by which the stars are known in the literature, taken from Lloyd-Evans (1980), Mighell et al. (1996), and LMC-O98.

The blue side of the double echelle design covers 3200–4800 Å, and the red, 4500–7240 Å, with no gaps. For the analyses presented here, we only employ the relatively higher signal-to-noise ($S/N > 20$) data redward of 4800 Å. We used a 1.0 arcsec wide slit, giving a spectral resolution of 19,000 ($R \equiv \lambda/\Delta\lambda$). The chip had a gain of 1.06 electrons/ADU and a read noise of 4 electrons. We binned on-chip in 2x2 pixels. Table 1 lists the S/N per pixel we achieved in the combined spectra at 6600 Å, along with a measure of the quality factor per resolution element ($F \equiv (R/\lambda) \times (S/N)$), also referred to as a figure-of-merit.

The data were reduced using standard IRAF⁶ routines. We also employed IRAF to combine multiple spectra taken of the same objects and to excise cosmic ray features. Spectra taken of Th-Ar lamps provided the wavelength calibration. We took several spectra of the hot, rapid rotator HR 1307 to eliminate the telluric features using a current version of the program SPECTRE (Fitzpatrick & Sneden 1987).

3. ABUNDANCE ANALYSIS

In this section we describe our analysis techniques. In the abundance determinations, we employed a combination of equivalent width and spectrum synthesis analyses.

⁶ IRAF is distributed by NOAO, which is operated by AURA, under cooperative agreement with the NSF.

Also presented here are the linelists we used, including hyperfine structure information (HFS) where applicable, and equivalent widths (EWs). We include a brief discussion of the effect of different choices in the stellar parameters on the derived abundances, and expand upon that discussion in the appendix.

3.1. Equivalent Widths

To identify transitions suitable for EW analyses, we synthesized the spectrum (4500–7240 Å) of NGC 1898#1 with a current version of MOOG (Sneden 1973) and identified relatively isolated lines stronger than ~ 25 mÅ. These features were then measured in each of our spectra using SPECTRE. For most species, including Ca I, Ti I, and Fe I, EW measurements were sufficient for a reliable abundance analysis. For other elements, some or all of the lines were synthesized. For these lines a pseudo-EW was calculated via the ewfind driver in MOOG for inclusion in Table 2. Table 2 lists the lines we employed in the abundance analyses. Pseudo-EWs are given for lines marked “SYN”.

The uncertainty in the EW for each line can be determined by the following relationship (corrected from Equation 3 in Fulbright & Johnson, 2003):

$$\delta EW^2 = \delta x^2 (\Sigma \delta r_i^2 + (n^2 - n + 1) \Sigma \delta C_i^2), \quad (1)$$

where δx is the dispersion in $\text{Å}/\text{pix}$, C_i is the value of the continuum, and r_i is the intensity at pixel i . This is summed over the n pixels which contain absorption in the line. In practice, we summed over $2.5 \times \text{FWHM}$ of the line, where the FWHM was given by the gaussian fit via SPECTRE.

The uncertainty in the continuum placement is difficult to determine. We employed the following procedure. We selected a subset of Ti and Fe lines with oscillator strengths from Wickliffe & Lawler (1997) and the papers of the Oxford group (Blackwell, Petford, & Shallis 1979; Blackwell et al. 1979; Blackwell, Petford, & Simmons 1982; Blackwell et al. 1982a, 1982b, 1982c; Blackwell et al. 1986). These oscillator strengths, especially in a relative sense, are well determined, with uncertainties of < 0.05 dex (which are smaller than the uncertainties imposed by the EW measurements). We varied the number of continuum pixels from 10 at 4500 Å to 25 at 7000 Å, values chosen based on our previous experience with high resolution spectral syntheses. With this algorithm, the average uncertainty in the abundance produced by the uncertainty in the EW is equal to the standard deviation of the sample of lines. We then determined the expected uncertainty for each individual EW.

Lines that were not significant at the $2\text{-}\sigma$ level were eliminated. The number of lines eliminated by this criterion varied from one to six per star. We also used Equation 1 to determine limits for certain species where only upper limits could be measured. The smallest uncertainty was then tripled and used to calculate an abundance based on a $3\text{-}\sigma$ upper limit.

3.2. Oscillator Strengths

Table 2 summarizes the oscillator strengths we employed. Whenever possible, we have chosen to employ laboratory values. In the appendix, we discuss the effect (usually small) on the abundances that choosing values

TABLE 1
LMC CLUSTER OBSERVATIONS

Star	Other Name	V (mag)	Obs. Date	Exposures	S/N	F ($\sim 6600 \text{ \AA}$)
NGC 1898#1	O8535	16.59	2002 Dec 31	3×2400s	70	319
NGC 1898#2	O8526	16.46	2003 Jan 1	3×1800s	50	228
NGC 2005#1	O9347	16.37	2002 Dec 28	2×3600s	70	319
NGC 2005#2	O9348	16.92	2003 Jan 1	3×1800s	40	182
NGC 2005#3	O9353	16.83	2002 Dec 30	3×2700s	35	159
NGC 2019#1	O9697	16.56	2002 Dec 29	3×2700s	45	205
NGC 2019#2	O9688	16.46	2002 Dec 31	3×2400s	65	296
NGC 2019#3	O9692	16.24	2002 Dec 28	1×3600s		
			2002 Dec 29	2×1800s	75	341
Hodge 11#1	Mighell	<16.61 ^a	2002 Dec 31	1×1800s		
	219234439	16.28 ^b	2003 Jan 1	1×1200s		
			2003 Jan 1	1×800s	45	205
Hodge 11#2	LE 2	16.61 ^b	2002 Dec 29	3×1800s	60	273

^aSaturated image. See § 2.1.

^bPhotometry from private catalog maintained by Stetson.

from other studies would make, and compare our oscillator strengths to those of the Lick-Texas Group (e.g., the linelist employed in the recent high resolution M3 study by Sneden et al. 2004 adopted from M5-I01) and the list of Shetrone et al. (2001; dSph-S01) for dSph stars, a list also incorporated into studies of additional metal-poor dSph stars by Shetrone et al. (2003) and further discussed by Tolstoy et al. (2003) and Venn et al. (2004).

In deriving the abundances of Sc, V, Mn, Co, Cu, Ba, La, and Eu, we took into account HFS for all of the lines we employed. The La and Eu linelists were taken from Lawler, Bonvallet & Sneden (2001) and Lawler et al. (2001); Ba from Johnson (2002); and Cu from Simmerer et al. (2003). In Table 3, we present our HFS information for the lines we analysed in Sc, V, Mn, and Co, where the integrated line information and references are listed in Table 2. In the case of Na and Al, our analyses are consistent with those in the literature where weak lines are used and HFS is ignored. Nd has eight isotopes and the odd-Z isotopes have HFS. We do not have information on the HFS, but using the Nd isotopic splittings from Aoki et al. (2001) did not make a difference, so the effect of saturation on the lines should be small. For all elements, we use van der Waals damping constants modified by the Unsöld approximation.

3.3. Model Atmospheres

We used Kurucz model atmospheres (Kurucz 1992, 1993)⁷ with overshooting and assumed that local thermodynamic equilibrium (LTE) holds for all species. In the appendix, we discuss the effect on our abundance calculations for different sets of model atmospheres.

Reliable photometry does not exist for all of the stars in our sample. We instead derived temperatures by ensuring that the abundance derived for Fe I lines did not show any trends with the atomic parameters of the lines employed. As shown by M5-I01 and Kraft & Ivans (2003; Fe-KI03 hereafter), in their sample of metal-poor GCs RGB stars, temperatures derived from the color-temperature calibrations of Alonso et al. (1999) seem to

be generally in good agreement with the excitation temperatures derived by spectroscopic means. The photometric temperatures we calculate for some of the LMC stars are generally cooler than those adopted here, and this issue is discussed further in the appendix. We estimate our uncertainty in T_{eff} to be 150K.

Our log g values are calculated from the following relationship:

$$\log g = \log \frac{M}{M_{\odot}} - 0.4(M_{\text{bol}}^{\odot} - M_V - BC) + 4 \log \frac{T_{\text{eff}}}{T_{\text{eff}}^{\odot}} + \log g_{\odot}, \quad (2)$$

where the bolometric correction (BC) was obtained by employing the formulae of Alonso et al. (1999). We adopted $T_{\text{eff}}^{\odot} = 5770 \text{ K}$, $\log g_{\odot} = 4.44$ and $M_{\text{bol}}^{\odot} = 4.72$. We also adopt $0.85M_{\odot}$ for the mass of our stars. Of the four different $(m-M)_V$ distance modulus calculations presented by LMC-O98, we used the apparent distance modulus they derived based on matching the color-magnitude diagrams of GCs to those of the LMC clusters. The values we derive employing this method are in good agreement with those predicted by the 12 Gyr, $Z = 10^{-4}$ isochrones of Bergbusch & Vandenberg (1992). In the case of Hodge 11, homogeneous photometry for the stars in this cluster did not initially exist, so we adopted the isochrone-based log g . Further discussion of these issues are contained in the appendix.

We determined the microturbulent velocity (ξ) spectroscopically by ensuring that there were no trends in the abundance of Fe I as a function of EW. Fe II was used for the input metallicity of the model atmosphere, $[m/H]$. Our final model atmosphere parameters are presented in Table 4.

3.4. Effect of Stellar Parameters on Derived Abundances

Our abundances are summarized in Tables 5–14. The stellar parameters we adopted result in a disagreement between the abundances of Fe II and Fe I, and Ti II and Ti I, with the lines of the ionized species producing

⁷ Grids of Kurucz model atmospheres can be downloaded from <http://cfaku5.cfa.harvard.edu/grids.html>.

TABLE 4
MODEL ATMOSPHERE PARAMETERS

Star	T_{eff}	$\log g$	ξ	[m/H]
NGC 1898#1	4050	0.70	2.1	-0.80
NGC 1898#2	4000	0.60	2.3	-0.80
NGC 2005#1	4050	0.61	2.1	-1.30
NGC 2005#2	4350	1.05	1.9	-1.30
NGC 2005#3	4250	0.95	2.0	-1.30
NGC 2019#1	4250	0.87	2.1	-1.10
NGC 2019#2	4050	0.68	2.0	-1.10
NGC 2019#3	3950	0.50	2.2	-1.10
Hodge 11#1	4300	0.66	2.2	-2.00
Hodge 11#2	4200	0.50	2.0	-2.00

TABLE 5
ABUNDANCES FOR NGC1898#1

Species	$\log \epsilon$	σ_{ϵ}	[X/Fe] ^a	$\sigma_{[X/Fe]}$	σ_{lines}	N_{lines}
O I	8.13	0.16	-0.05	0.32	0.07	2
Na I	4.58	0.18	-0.49	0.22	0.10	2
Mg I	6.44	0.25	0.12	0.21	0.29	2
Si I	6.59	0.15	0.30	0.21	0.14	4
Ca I	4.90	0.28	-0.20	0.20	0.16	15
Sc II	2.02	0.20	-0.33	0.32	0.16	2
Ti I	3.48	0.20	-0.25	0.29	0.20	33
Ti II	4.03	0.18	-0.21	0.29	0.15	7
V I	2.24	0.30	-0.50	0.31	0.14	14
Cr I	4.19	0.29	-0.22	0.23	0.25	8
Mn I	3.69	0.17	-0.44	0.17	0.08	5
Fe I	6.26	0.19	-1.26	...	0.20	145
Fe II	6.77	0.36	0.51	0.35	0.21	6
Co I	3.61	0.09	-0.05	0.15	0.12	10
Ni I	4.91	0.17	-0.08	0.10	0.28	20
Cu I	2.11	0.14	-0.84	0.13	0.11	2
Y II	0.76	0.19	-0.22	0.15	0.22	4
Zr I	0.99	0.34	-0.35	0.36	0.11	3
Ba II	1.17	0.37	0.30	0.27	0.27	2
La II	0.18	0.11	0.22	0.18	0.11	2
Nd II	0.75	0.18	0.51	0.10	0.11	6
Eu II	-0.27	0.15	0.48	0.21	0.10	1

^a[X/Fe] given for each species except for Fe I, when [Fe I/H] is given

larger values for $\log \epsilon(X)$ by 0.3–0.5 dex. Non-LTE effects could account for the difference, if the neutral species are “over-ionized” due to the models employed (see Fe-KI03 for an expanded discussion). However, the magnitude of the over-ionization effect is not predicted to be as large as this (Gratton et al. 1999, Korn 2004). Further discussion regarding these issues is postponed to the appendix.

In Figure 2, we illustrate the changes in $\log \epsilon(X)$ due to the estimated uncertainties in each of the stellar parameters for NGC 1898#1, a representative star from our sample. For our particular set of Fe I and Fe II lines, most of the elemental abundances changes behave in a similar way to the changes observed in Fe I. In subsequent discussions, we reference all abundances with respect to Fe I, except for O I, Ti II, and Sc II, which are referenced to Fe II. Our choice of whether to compare to Fe I or Fe II was based on the relative changes when atmospheric parameters were changed, as were the sizes of possible NLTE effects and the ratios that have previously been used in the literature. Our error analysis is

TABLE 6
ABUNDANCES FOR NGC1898#2

Species	$\log \epsilon$	σ_{ϵ}	[X/Fe] ^a	$\sigma_{[X/Fe]}$	σ_{lines}	N_{lines}
Na I	5.16	0.24	0.02	0.17	0.11	2
Mg I	6.33	0.20	-0.06	0.12	0.15	2
Al I	6.05	0.18	0.77	0.16	0.10	2
Si I	6.72	0.16	0.36	0.24	0.15	3
Ca I	5.00	0.32	-0.17	0.19	0.16	13
Sc II	2.18	0.16	-0.05	0.36	0.19	6
Ti I	3.59	0.34	-0.21	0.26	0.22	30
Ti II	4.13	0.22	0.01	0.29	0.29	5
V I	2.40	0.33	-0.41	0.27	0.15	13
Cr I	4.29	0.31	-0.19	0.20	0.16	7
Mn I	3.72	0.18	-0.48	0.14	0.13	5
Fe I	6.33	0.18	-1.19	...	0.24	131
Fe II	6.65	0.32	0.32	0.37	0.28	4
Co I	3.56	0.11	-0.17	0.15	0.18	8
Ni I	4.93	0.17	-0.13	0.10	0.20	17
Cu I	2.21	0.17	-0.81	0.14	0.14	2
Y II	0.81	0.24	-0.24	0.20	0.36	4
Zr I	1.20	0.34	-0.21	0.30	0.07	3
Ba II	1.43	0.37	0.49	0.24	0.20	2
La I	0.23	0.12	0.20	0.19	0.13	2
Nd II	0.89	0.25	0.58	0.16	0.32	6
Eu II	-0.24	0.14	0.44	0.23	0.10	1

^a[X/Fe] given for each species except for Fe I, when [Fe I/H] is given

TABLE 7
ABUNDANCES FOR NGC2005#1

Species	$\log \epsilon$	σ_{ϵ}	[X/Fe] ^a	$\sigma_{[X/Fe]}$	σ_{lines}	N_{lines}
O I	7.68	0.16	0.10	0.30	0.10	1
Na I	4.58	0.19	-0.06	0.16	0.07	2
Mg I	6.00	0.28	0.11	0.24	0.34	2
Ca I	4.61	0.28	-0.06	0.18	0.15	14
Sc II	1.76	0.17	0.01	0.28	0.18	5
Ti I	3.04	0.33	-0.26	0.27	0.12	16
Ti II	3.72	0.19	0.08	0.26	0.21	5
V I	1.75	0.35	-0.56	0.32	0.14	9
Cr I	3.64	0.38	-0.34	0.26	0.06	4
Mn I	3.06	0.23	-0.64	0.19	0.06	3
Fe I	5.83	0.16	-1.69	...	0.19	111
Fe II	6.21	0.33	0.37	0.37	0.17	4
Co I	3.08	0.12	-0.15	0.13	0.15	5
Ni I	4.33	0.15	-0.23	0.10	0.29	14
Cu I	1.51	0.12	-1.01	0.14	0.07	1
Y II	0.36	0.14	-0.19	0.14	0.13	3
Ba II	0.71	0.31	0.27	0.21	0.16	2
La II	-0.18	0.17	0.29	0.20	0.15	1
Nd II	-0.12	0.25	0.07	0.24	0.32	2
Eu II	-0.72	0.18	0.46	0.23	0.15	1

^a[X/Fe] given for each species except for Fe I, when [Fe I/H] is given

described in detail in the appendix. The uncertainties in $\log(\epsilon)$ and in [X/Fe], including the effects of the model atmosphere uncertainties, are listed in Tables 5–14, along with the standard error of the sample for the abundances derived from different lines of the same element (σ_{lines}).

4. DISCUSSION: ABUNDANCE RESULTS

4.1. [Fe/H]

In Table 15, we compare our values for [Fe/H] in these clusters from Fe I and Fe II lines with those from the

TABLE 8
 ABUNDANCES FOR NGC2005#2

Species	$\log \epsilon$	σ_ϵ	$[X/Fe]^a$	$\sigma_{[X/Fe]}$	σ_{lines}	N_{lines}
Mg I	6.09	0.22	0.37	0.15	0.23	3
Ca I	4.73	0.28	0.23	0.10	0.20	12
Ti I	3.21	0.35	0.08	0.23	0.31	6
Ti II	4.02	0.26	0.35	0.36	0.25	3
Fe I	5.66	0.23	-1.86	...	0.27	75
Fe II	6.20	0.37	0.54	0.46	0.37	2
Ni I	4.37	0.23	-0.02	0.16	0.45	9
Sc II	1.66	0.14	-0.12	0.34	0.08	4
Mn I	2.96	0.43	-0.57	0.31	0.29	2
Ba II	0.77	0.31	0.50	0.26	0.19	2

^a $[X/Fe]$ given for each species except for Fe I, when $[Fe I/H]$ is given

 TABLE 9
 ABUNDANCES FOR NGC2005#3

Species	$\log \epsilon$	σ_ϵ	$[X/Fe]^a$	$\sigma_{[X/Fe]}$	σ_{lines}	N_{lines}
Na I	4.47	0.19	0.00	0.15	0.07	1
Mg I	5.90	0.20	0.18	0.14	0.19	3
Ca I	4.65	0.28	0.15	0.13	0.17	12
Sc II	1.51	0.17	-0.22	0.25	0.21	4
Ti I	3.08	0.34	-0.05	0.24	0.14	8
Ti II	3.55	0.19	-0.07	0.25	0.28	5
Cr I	3.80	0.38	-0.01	0.25	0.39	5
Mn I	2.93	0.30	-0.60	0.24	0.23	5
Fe I	5.66	0.21	-1.86	...	0.27	91
Fe II	6.15	0.28	0.49	0.37	0.21	6
Co I	2.96	0.17	-0.10	0.14	0.07	2
Ni I	4.24	0.18	-0.15	0.13	0.35	11
Cu I	1.57	0.17	-0.78	0.15	0.11	2
Y II	0.39	0.16	0.01	0.20	0.14	2
Ba II	0.72	0.38	0.45	0.29	0.21	1
Nd II	0.03	0.13	0.39	0.18	0.15	3

^a $[X/Fe]$ given for each species except for Fe I, when $[Fe I/H]$ is given

literature. Our value of $[Fe/H]$ for Hodge 11 is in good agreement with previous literature estimates, as is the value we derive for NGC 1898. We find both NGC 2005 and NGC 2019 to be more metal-rich than the previous estimates by LMC-O91 from the Ca II triplet. Instead, we derive $[Fe/H]$ values closer to those obtained by LMC-O98 from the slope of the red giant branch. LMC-O91 specifically noted problems with their analysis of these two clusters. In each case, LMC-O91 could rely on only one star in the center of the cluster. Our analysis shows that both of these clusters are closer in metallicity to NGC 1898 than to Hodge 11. Therefore Figure 17 from LMC-O98 is substantially correct: the inner LMC clusters are more metal-rich than the outer LMC clusters even though both have similar horizontal branch (HB) morphologies. HB morphology is mainly a function of metallicity, and more metal-rich clusters have redder HBs. That metallicity is not the sole variable affecting HB morphology is referred to as the “second-parameter problem” (van den Bergh 1967). In the Milky Way, Searle & Zinn (1978) pointed out that the clusters with bluer HBs (for their metallicity) are concentrated within 8 kpc of the Galactic Center, while the

 TABLE 10
 ABUNDANCES FOR NGC2019#1

Species	$\log \epsilon$	σ_ϵ	$[X/Fe]^a$	$\sigma_{[X/Fe]}$	σ_{lines}	N_{lines}
O I	8.08	0.09	0.41	0.27	0.00	2
Na I	4.68	0.22	-0.36	0.20	0.21	2
Mg I	6.57	0.21	0.28	0.09	0.12	2
Si I	7.10	0.10	0.84	0.21	0.00	1
Ca I	5.17	0.29	0.10	0.13	0.16	15
Sc II	1.91	0.17	0.07	0.27	0.21	4
Ti I	3.86	0.34	0.16	0.25	0.18	21
Ti II	3.88	0.24	0.15	0.30	0.36	4
V I	2.61	0.36	-0.10	0.28	0.14	13
Cr I	4.44	0.31	0.06	0.17	0.20	7
Mn I	3.71	0.28	-0.39	0.17	0.13	3
Fe I	6.23	0.19	-1.29	...	0.23	129
Fe II	6.26	0.28	0.03	0.37	0.27	4
Co I	3.63	0.16	0.00	0.14	0.20	8
Ni I	4.94	0.21	-0.02	0.11	0.37	14
Cu I	2.21	0.19	-0.71	0.13	0.14	2
Y II	0.99	0.21	0.04	0.20	0.21	2
Zr I	1.57	0.39	0.26	0.31	0.03	3
Ba II	1.13	0.32	0.29	0.22	0.13	2
Nd II	0.83	0.19	0.62	0.13	0.14	5
Eu II	-0.12	0.19	0.66	0.27	0.17	1

^a $[X/Fe]$ given for each species except for Fe I, when $[Fe I/H]$ is given

 TABLE 11
 ABUNDANCES FOR NGC2019#2

Species	$\log \epsilon$	σ_ϵ	$[X/Fe]^a$	$\sigma_{[X/Fe]}$	σ_{lines}	N_{lines}
O I	7.93	0.18	0.03	0.35	0.13	1
Na I	4.73	0.20	-0.18	0.21	0.14	2
Al I	5.07	0.18	0.02	0.19	0.10	1
Mg I	6.60	0.17	0.44	0.07	0.08	2
Ca I	4.97	0.29	0.03	0.19	0.24	15
Sc II	1.87	0.17	-0.20	0.33	0.12	4
Ti I	3.57	0.33	0.00	0.29	0.16	27
Ti II	4.16	0.23	0.20	0.33	0.30	6
V I	2.24	0.34	-0.34	0.32	0.21	14
Cr I	4.21	0.29	-0.04	0.22	0.22	8
Mn I	3.59	0.19	-0.38	0.18	0.07	3
Fe I	6.10	0.18	-1.42	...	0.23	127
Fe II	6.58	0.40	0.48	0.41	0.35	4
Co I	3.48	0.11	-0.02	0.16	0.15	5
Ni I	4.67	0.16	-0.16	0.09	0.20	18
Cu I	2.06	0.16	-0.73	0.14	0.14	2
Y II	0.97	0.45	0.15	0.40	0.00	1
Zr I	1.28	0.42	0.10	0.40	0.06	2
Ba II	0.88	0.32	0.17	0.19	0.05	2
La II	0.15	0.25	0.35	0.28	0.33	2
Nd II	0.67	0.21	0.59	0.15	0.24	4
Eu II	-0.06	0.14	0.85	0.21	0.08	1

^a $[X/Fe]$ given for each species except for Fe I, when $[Fe I/H]$ is given

clusters with redder HBs lie at larger distances. With our confirmation of the higher metallicities of the inner LMC clusters, it appears that the LMC clusters exhibit second-parameter effects that mimic those of the GGCs.

4.2. Literature Sources for Comparison with Abundance Ratios

One of the primary goals of this paper is to compare the LMC cluster abundance ratios with those seen in other

TABLE 12
ABUNDANCES FOR NGC2019#3

Species	$\log \epsilon$	σ_ϵ	$[X/Fe]^a$	$\sigma_{[X/Fe]}$	σ_{lines}	N_{lines}
O I	7.81	0.11	-0.01	0.37	0.06	1
Na I	4.90	0.19	-0.03	0.21	0.04	2
Mg I	6.41	0.17	0.23	0.08	0.08	2
Si I	6.53	0.14	0.38	0.20	0.07	3
Ca I	4.94	0.28	-0.02	0.21	0.20	14
Sc II	1.77	0.18	-0.22	0.38	0.18	4
Ti I	3.59	0.32	0.00	0.31	0.21	29
Ti II	4.23	0.28	0.35	0.40	0.51	7
V I	2.32	0.32	-0.28	0.33	0.17	14
Cr I	4.24	0.32	-0.03	0.25	0.28	6
Mn I	3.49	0.17	-0.50	0.19	0.14	5
Fe I	6.12	0.18	-1.40	...	0.23	129
Fe II	6.41	0.42	0.29	0.41	0.37	4
Co I	3.35	0.10	-0.17	0.16	0.18	8
Ni I	4.78	0.17	-0.07	0.10	0.27	17
Cu I	1.98	0.17	-0.83	0.17	0.18	2
Zr I	1.40	0.36	0.20	0.42	0.13	2
Ba II	1.09	0.36	0.36	0.23	0.19	2
La II	0.27	0.17	0.45	0.16	0.22	4
Nd II	0.97	0.44	0.87	0.35	0.35	4
Eu II	-0.03	0.13	0.86	0.19	0.07	1

^a $[X/Fe]$ given for each species except for Fe I, when $[Fe I/H]$ is given

TABLE 13
ABUNDANCES FOR HODGE 11#1

Species	$\log \epsilon$	σ_ϵ	$[X/Fe]^a$	$\sigma_{[X/Fe]}$	σ_{lines}	N_{lines}
Mg I	5.84	0.24	0.47	0.16	0.19	3
Ca I	4.41	0.26	0.26	0.12	0.18	12
Ti I	2.69	0.49	-0.09	0.27	0.25	2
Ti II	3.48	0.41	0.60	0.42	0.38	1
Cr I	3.43	0.47	-0.03	0.21	0.15	3
Fe I	5.30	0.31	-2.22	...	0.26	49
Fe II	5.41	0.18	0.11	0.40	0.20	3
Ni I	3.87	0.29	-0.17	0.17	0.25	4
Sc II	1.18	0.17	0.19	0.22	0.25	3
Mn I	2.65	0.64	-0.53	0.51	0.46	1
Eu II	-0.35	0.10	1.35	0.29	0.09	1
Ba II	0.00	0.23	0.08	0.24	0.13	2

^a $[X/Fe]$ given for each species except for Fe I, when $[Fe I/H]$ is given

stellar populations. The sample of recent literature studies of the GGCs used for comparison in this paper is summarized in Table 16. For Cu, we used the comprehensive analysis of Simmerer et al. (2003) for the GGCs values. For the elements sensitive to proton-capture nucleosynthesis (e.g., O, Na, Mg, and Al), we have displayed the abundances from individual stars. For all other elements, as well as Mg, we have adopted or calculated the average abundance and standard error of the mean (s.e.m.). Using the s.e.m. usually gives us a very small (~ 0.03) error, much smaller than we calculate for the individual errors in the LMC stars. Much of the reduction comes from the large number of stars observed in GCC studies. Some of the reduction, however, is the result of the usually smaller internal dispersions in globular cluster abundance ratios where the determinations of the relative T_{eff} and $\log g$ values are more secure. The $[Fe/H]$ values pre-

TABLE 14
ABUNDANCES FOR HODGE 11#2

Species	$\log \epsilon$	σ_ϵ	$[X/Fe]^a$	$\sigma_{[X/Fe]}$	σ_{lines}	N_{lines}
Mg I	5.82	0.25	0.44	0.14	0.13	4
Ca I	4.49	0.30	0.33	0.13	0.12	14
Sc II	1.11	0.11	0.00	0.24	0.18	6
Ti I	2.80	0.47	0.01	0.25	0.21	4
Ti II	3.35	0.16	0.35	0.24	0.23	5
Cr I	3.46	0.50	-0.01	0.30	0.43	4
Mn I	2.39	0.47	-0.80	0.26	0.10	1
Fe I	5.32	0.28	-2.20	...	0.21	79
Fe II	5.53	0.25	0.21	0.43	0.40	5
Co I	2.77	0.29	0.05	0.14	0.08	3
Ni I	3.92	0.27	-0.13	0.15	0.34	11
Y II	0.09	0.19	0.05	0.31	0.26	3
Ba II	0.02	0.25	0.09	0.26	0.08	2

^a $[X/Fe]$ given for each species except for Fe I, when $[Fe I/H]$ is given

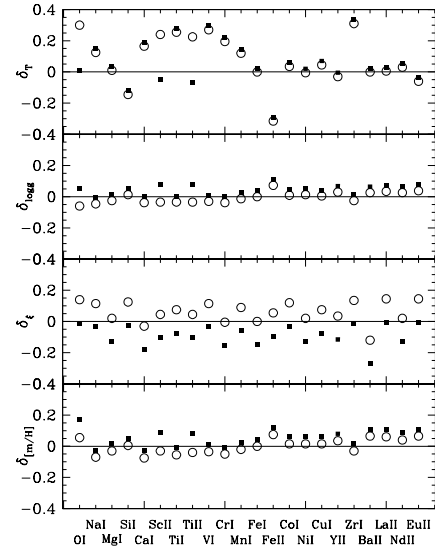


FIG. 2.— The changes in $\log \epsilon(X)$ (filled squares) and $[X/Fe]$ (open circles) for NGC 1898#1 for the different species included in our study. The ratio $[X/Fe]$ has been taken with respect to Fe I for all elements except O I, Sc II, and Ti II, which are taken with respect to Fe II. Fe is taken with respect to H. We varied T_{eff} , $\log g$, ξ and $[m/H]$ individually to produce these plots. The δ values represent changes to T_{eff} by 150K, $\log g$ by 0.2 dex, ξ by 0.3 km/s and $[m/H]$ by 0.3 dex. Such dependences as the abundance from Fe II lines on the T_{eff} and the abundance from Ba II lines on ξ are readily apparent. The large decrease in the Fe I abundance when ξ is increased results in a uniform increase in the $[X/Fe]$ values in the third panel.

sented here for the GGCs are from Fe-KI03 (Tables 4 and 7) and Kraft & Ivans (2004; Fe-KI04), where available, using $[Fe/H]$ derived from Kurucz atmospheres with overshooting turned on, corresponding to the choice made for this study. For Terzan 7 and NGC 6553, too metal-rich to be included in the Fe-KI03 and Fe-KI04 compilations, we cite the $[Fe/H]$ reported in primary abundance analyses in the literature. The abundance analyses for 18 of these clusters were done using evolutionary $\log g$ values; the other seven adopted $\log g$ based on ionization equilibrium. In studies where these two methods were compared (e.g., M5-I01), the $\log g$ values for stars at

TABLE 15
[Fe/H] COMPARISON

Cluster	[Fe/H]	Source	Technique
Hodge 11	-2.21	This Study	High-Res Spectra Fe I
	-2.05	This Study	High-Res Spectra Fe II
	-2.1	LMC-CH	Low-Res Indices
	-2.0	Walker (1993)	Color of RGB
NGC 1898	-1.23	This Study	High-Res Spectra Fe I
	-0.81	This Study	High-Res Spectra Fe II
	-1.37	LMC-O91	Low-Res Ca II Triplet
NGC 2005	-1.18	LMC-O98	Slope of RGB
	-1.47	This Study	High-Res Spectra Fe I
	-1.33	This Study	High-Res Spectra Fe II
NGC 2019	-1.92	LMC-O91	Low-Res Ca II Triplet
	-1.35	LMC-O98	Slope of RGB
	-1.37	This Study	High-Res Spectra Fe I
	-1.10	This Study	High-Res Spectra Fe II
	-1.81	LMC-O91	Low-Res Ca II Triplet
	-1.23	LMC-O98	Slope of RGB

TABLE 16
LITERATURE SOURCES FOR GALACTIC GLOBULAR CLUSTERS

Cluster	Source	[Fe/H]	#
M3	Sneden et al. 2004	-1.42	23
M4	Ivans et al. 1999	-1.08	36
M5	Ivans et al. 2001	-1.19	36
M10	Kraft et al. 1995	-1.43	15
M13	Sneden et al. 2004	-1.52	35
M15	Sneden et al. 1997	-2.36	18
M54	Brown, Wallerstein, & Gonzalez 1999	-1.40	5
M68	Lee et al. 2004	-2.37	7
M71	Ramírez & Cohen 2002	-0.74	25
NGC 288	Shetrone & Keane 2000	-1.27	13
NGC 362	Shetrone & Keane 2000	-1.33	12
NGC 2808	Carretta, Bragaglia & Cacciari 2004	-1.22	20
NGC 3201	Gonzalez & Wallerstein 1998	-1.48	18
NGC 6287	Lee & Carney 2002	-2.13	3
NGC 6293	Lee & Carney 2002	-1.97	2
NGC 6397	Gratton et al. 2001	-1.96	8
NGC 6541	Lee & Carney 2002	-1.76	2
NGC 6752	Gratton et al. 2001	-1.49	18
NGC 6752	James et al. 2004	-1.49	18
NGC 7006	Kraft et al. 1998	-1.40	6
NGC 6553	Cohen et al. 1999	-0.18 ^a	5
47Tuc	Carretta et al. 2004	-0.63	12
Pal 5	Smith, Sneden, & Kraft 2002	-1.34 ^a	4
Pal 12	Cohen 2004	-0.87	3
Terzan 7	Tautvaišienė et al. 2004	-0.61 ^a	3

^aToo metal-rich to have been included by Fe-KI03 or Fe-KI04; adopted from source.

the tip of the giant branch from ionization equilibrium constraints are ~ 0.3 dex smaller than those derived from evolutionary considerations. From Figure 2, this will result in small changes (< 0.05 dex) for the majority of abundance ratios, with the exception of [Fe I/Fe II].

We did not apply any corrections to Na I abundances for non-LTE effects but took care to employ a similar sample for comparison, revising the values of two groups by the corresponding cited corrections (Tautvaišienė et

al. 2004; Carretta et al. 2004b). On this issue, we refer the reader to discussions by Baumüller, Butler, & Gehren (1998), Gratton et al. (1999), Mashonkina, Shimanskiĭ, & Sakhিবullin (2000), and Takeda et al. (2003).

For field star data, we have mainly relied on the work of Fulbright (2000). For elements not studied by Fulbright, we have adopted Sc and Co from Gratton & Sneden (1991), and Mn from Gratton (1989) and Bai et al. (2004). The data for Cu in field stars is from Mishenina et al. (2002). All of the additional field star studies for these elements include HFS in their analysis. The EWs for V in Fulbright (2000) are small enough that including HFS effects will not affect the derived values. The dSph field star data come from Shetrone et al. (2003), McWilliam, Rich, & Smecker-Hane (2003), Smecker-Hane & McWilliam (2004), Geisler et al. (2004), and McWilliam & Smecker-Hane (2005).

With the exception of iron, our analysis relies on the solar photospheric (where reliable) or meteoritic abundances from the compilation of Anders & Grevesse (1989). In the case of iron, we adopt $\log \epsilon(\text{Fe}) = 7.52$, a value close to that recommended by Grevesse & Sauval (1998; $\log \epsilon(\text{Fe}) = 7.50$). We refer the reader to discussions by Ryan, Norris & Beers (1996) and McWilliam (1997), where some of the alternative solar iron abundance choices are summarized. In cases where the literature studies employed a solar value different from that adopted in this study, we adjusted their abundances to our system. The case where this revision made the most noticeable difference to our comparison was to the Co values of Gratton & Sneden (1991). When applied to solar EWs, the linelist we employ in this study reproduces within acceptable errors the solar abundances we adopted for all elements.

4.3. O, Na, Mg, Al

In all GGCs for which star-to-star abundance variations have been investigated for correlations between the abundances of elements sensitive to proton-capture nucleosynthesis, they have been found. In Figure 3, we display the abundances of [O/Fe] vs. [Na/Fe] and [Al/Fe] vs. [Al/Fe] for our LMC cluster stars along with results from GGCs. Very low O/high Na stars do not exist in our sample. Two of our stars, NGC 1898#2 and NGC 2019#2, have only upper limits for oxygen. However, NGC 1898#2 is also Al-rich, and thus may be a candidate star for deep mixing. Overall, the bright giants in our sample of LMC clusters resemble stars in clusters like M3 and the halo field, rather than stars in clusters like M13. It is unclear if we should even expect to see Na values as extreme as those in some of the GGCs – the LMC stars may have been born with lower [Na/Fe] values. Smith et al. (2002) found that the LMC stars, in general, had lower [Na/Fe] values than those in the Milky Way field.

4.4. α elements

As seen in Figure 3, [O/Fe] in most of our sample is at the lower boundary of [O/Fe] observed in GGC stars. In Figure 4, we show the ratios for other α elements, [Mg/Fe], [Si/Fe], [Ca/Fe], and [Ti/Fe], compared to stars of the Galactic halo field, LMC, the dSphs and GGCs. While the [Mg/Fe] and [Si/Fe]-ratios we derived

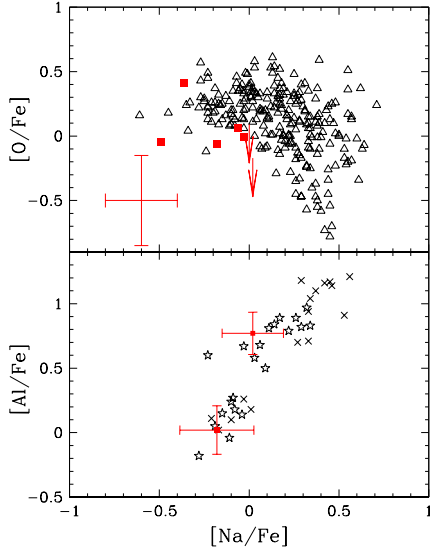


FIG. 3.— (top) $[\text{Na}/\text{Fe}]$ vs. $[\text{O}/\text{Fe}]$ for individual stars in the LMC (solid squares and limits) and the GGCs (open triangles; see Table 16 for sources). A typical error bar is shown the lower left. (bottom) $[\text{Al}/\text{Fe}]$ vs. $[\text{Na}/\text{Fe}]$ for LMC stars (solid squares) compared with M3 stars (stars) and M13 stars (crosses). Two LMC stars from our sample possess both Al and Na measurements.

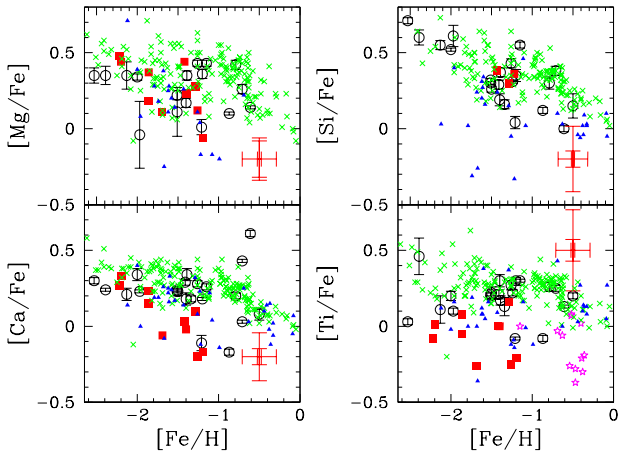


FIG. 4.— $[\text{Mg}/\text{Fe}]$, $[\text{Si}/\text{Fe}]$, $[\text{Ca}/\text{Fe}]$, and $[\text{Ti}/\text{Fe}]$ vs. $[\text{Fe}/\text{H}]$ for individual stars in the LMC clusters (solid squares) and dSph (solid triangles), for field stars in the Milky Way (crosses), for stars in GGCs (open circles), and for the LMC field (stars; Smith et al. 2002). The double error bar represents our estimate of total and random errors. The larger errorbar represents the uncertainty including atmosphere parameter uncertainties, and the smaller the addition of the s.e.m. from the lines of the two elements added in quadrature for the vertical axis or just the s.e.m. for the horizontal. The latter errorbars are similar to the errorbars of the GGCs. In the case of the larger Ti errors, the Ti line strengths, and thus derived abundances, are more temperature-sensitive than the other elements.

are in good agreement with those found for field and GGC stars, both the $[\text{Ca}/\text{Fe}]$ and $[\text{Ti}/\text{Fe}]$ ratios are systematically lower, with a distribution much more similar to the abundances found in some of the dSph stars.

4.5. Iron-peak elements

Two general abundance trends are observed in the iron-peak elements for Galactic field stars. At $[\text{Fe}/\text{H}] < -2.5$, there are trends with $[\text{Cr}/\text{Fe}]$ and $[\text{Mn}/\text{Fe}]$ decreasing

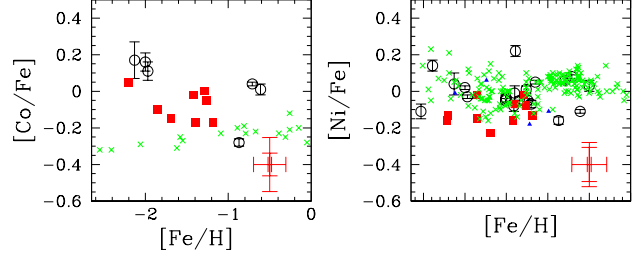


FIG. 5.— $[\text{Co}/\text{Fe}]$ and $[\text{Ni}/\text{Fe}]$ for individual stars in the LMC clusters (solid squares) compared with MW field stars (crosses) and average values in GGCs (open circles with error bars). A typical error bar for our data is shown. As noted in § 4.5, there is a paucity of comparison data for Co in the metallicity range of interest here.

as with decreasing $[\text{Fe}/\text{H}]$. For higher metallicities (and the only metallicities for which there are GGCs), all the iron-peak ratios, $[\text{Sc}, \text{V}, \text{Cr}, \text{Mn}, \text{Ni}/\text{Fe}]$, are essentially solar and show no trend with $[\text{Fe}/\text{H}]$. A few studies have argued for deviations from solar ratios, such as the super-solar $[\text{V}/\text{Fe}]$ found in some thick disk stars (Prochaska et al. 2000), and the low $[\text{V}/\text{Fe}]$ found in GGC Pal 12 stars (Cohen 2004).

Abundances of $[\text{Co}/\text{Fe}]$ and $[\text{Ni}/\text{Fe}]$, the heavier iron-peak elements, are displayed in Figure 5. The $[\text{Ni}/\text{Fe}]$ -values we derive in the LMC are lower than the average values within the GGCs, and are comparable to the lower Ni values observed in some dSph and low-Ni GCC stars. However, individual values agree, within the errors, to those of the GCC cluster and field stars. The abundance we derive for Co for the LMC clusters is offset from most of the GCC abundances displayed in Figure 5. However, as the errorbar illustrates, the offset could be the result of systematic choices in the analyses. We have excluded the Co abundances from the following discussion. We do, however, note the disagreement between the abundances reported for metal-poor field and GCC stars as well as the need for additional measurements of Co in metal-poor field stars.

Figure 6 shows the abundances of the lighter iron-peak elements, $[\text{Sc}/\text{Fe}]$, $[\text{V}/\text{Fe}]$, $[\text{Cr}/\text{Fe}]$, and $[\text{Mn}/\text{Fe}]$. While $[\text{Sc}/\text{Fe}]$, $[\text{Cr}/\text{Fe}]$ and $[\text{Mn}/\text{Fe}]$ all agree with the trends seen in the Milky Way, both field and clusters, the $[\text{V}/\text{Fe}]$ ratio in the LMC clusters is decidedly lower. $[\text{V}/\text{Fe}]$ is very sensitive to temperature, but so are other ratios in this group, such as $[\text{Cr}/\text{Fe}]$. Even by experimenting with the stellar parameters, we cannot find temperatures that force all the iron-peak ratios to have solar values. This aspect is illustrated further in the appendix.

4.6. Cu

The sites for Cu production are thought to be massive stars either through the weak *s*-process or Type II SNe, or lower mass binaries through Type Ia SNe (e.g., Matteucci et al. 1993). Whatever the relative contributions of these processes, they are also responsible for the strong trend seen in $[\text{Cu}/\text{Fe}]$ vs. $[\text{Fe}/\text{H}]$ in the field stars (Snedden & Crocker 1988; Mishenina et al. 2002), a trend also shared by the GGCs (Simmerer et al. 2003; their Figure 6), but not by the individual stars in ω Cen (Cunha et al. 2002). As shown in our Figure 7, the LMC clusters, like ω Cen, show no trend in $[\text{Cu}/\text{Fe}]$ with $[\text{Fe}/\text{H}]$. The Cu abundances and behavior with $[\text{Fe}/\text{H}]$ in the stars of ω Cen, the LMC, and the dSph systems all appear to be

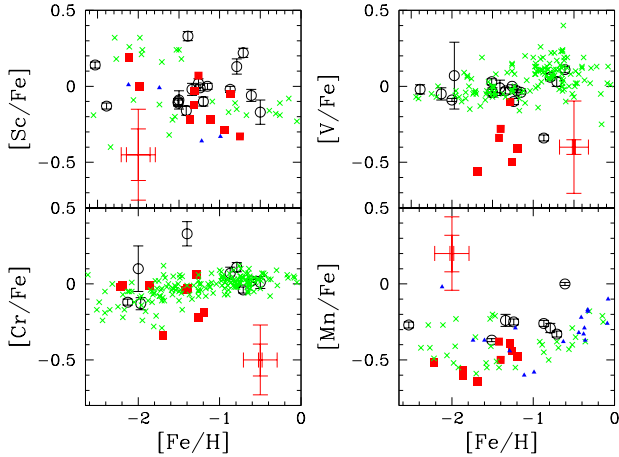


FIG. 6.— Abundance ratios for the iron-peak elements in individual stars in the LMC clusters (solid squares) compared with MW field stars (crosses), and average values in GGCs (open circles with error bars). A typical error bar for our data is shown. With the prominent exception of V, the iron-peak trends are in good agreement with the Milky Way trends. V, like Ti, is very temperature-sensitive but the error bars displayed here incorporate *both* random and systematic uncertainties.

similar to each other but significantly different from the trends and values observed in Milky Way field star or GCC populations.

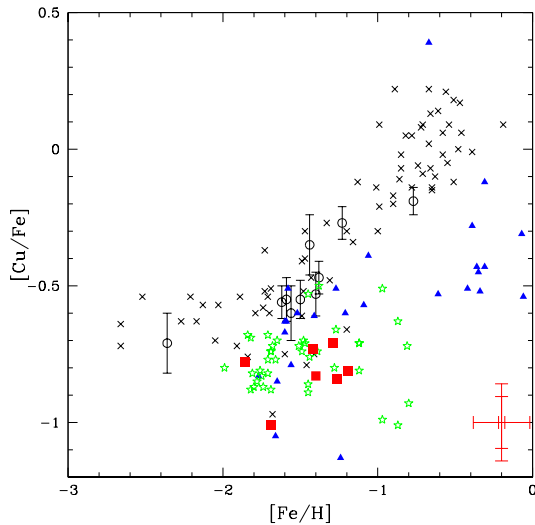


FIG. 7.— $[\text{Cu}/\text{Fe}]$ vs. $[\text{Fe}/\text{H}]$ for individual stars of the LMC (solid squares) and dSph systems (solid triangles), in the field of the Milky Way (crosses), the GGCs (open circles) and ω Cen (stars; Cunha et al. 2002). The GGC Cu values are those plotted in Figure 6 of Simmerer et al. (2003). Note that the halo field stars have slightly larger error bars than those of our study (see Figure 4).

4.7. Neutron-capture elements

In the solar system, Eu was mostly made in the r -process, while more than 50% of Y, Zr, Ba, La, and Nd came from the s -process. These two processes occur, and contribute to the interstellar mix out of which subsequent generations are formed, on different timescales. While the site of the r -process is not yet definitively known, the oldest stars in the Galaxy show the signature of r -process contributions, so a neutron-rich environment associated

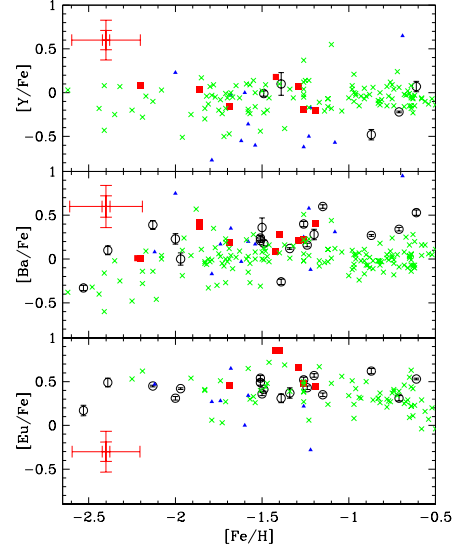


FIG. 8.— The abundance of three neutron-capture elements in giants in the LMC clusters (solid squares) compared with GGCs (open circles), and Galactic field stars (crosses), and dSph stars (triangles). The LMC clusters have similar enhancements to the GGCs and field stars in $[\text{Y}, \text{Ba}, \text{Eu}/\text{Fe}]$.

with massive stars is likely (Truran 1981). The s -process, however, is known to occur in AGB stars, and most efficiently in the lower-mass AGB stars (see e.g., the review by Busso, Gallino, & Wasserburg 1999 and references therein). Therefore, s -process material should appear in our clusters if they were formed out of material that had incorporated the yields of stars which had formed at least 1 Gyr previously. We measured six neutron-capture elemental abundances in both NGC 2019 and NGC 1898, and at least one neutron-capture element abundance in the other two clusters.

Figure 8 compares the abundance ratios for Y, Ba and Eu in the LMC clusters with those from the GGCs, the Milky Way field and the dSphs. First, the LMC clusters agree in general with the Milky Way field in all three ratios. Second, the Milky Way system shows large variations in $[\text{Ba}/\text{Fe}]$, as M4-I99 and M5-I01 show. Our smaller LMC sample does not include any examples of the extreme cases observed in the GGCs. Venn et al. (2004) noted that the dSph systems have a large number of stars with $[\text{Y}/\text{Fe}]$ substantially lower than the Galaxy and argued that this was due to a lower contribution of Y (but not Ba or Eu) from the r -process. Figure 8 shows that the LMC clusters do not share that trend.

5. THE CHEMICAL HISTORY OF THE LMC CLUSTERS

The LMC clusters in our sample do not show the same abundance ratios that we see in the majority of the GGCs. To determine if Type Ia SNe ejecta could be an explanation for the observed LMC $[\alpha/\text{Fe}]$ patterns, we compared the chemical abundances of three stars in two LMC clusters to supernova model yields. Table 17 lists the results, along with a subset of those obtained for other stars employing the same techniques, adapted from Table 12 of Ivans et al. (2003). The value of $\langle N_{\text{Ia}}/N_{\text{II}} \rangle$ represents the ratio of the number of SNe Ia to SNe II events that fit both the observations and the synthesized mass of Na, Mg, Si, and Fe from the model yields.

TABLE 17
SNE RATIOS DERIVED FROM STELLAR ABUNDANCE
FITS TO SN MODEL YIELDS

Population	$\langle N_{Ia}/N_{II} \rangle$		Ref.
	Source ^(a)	Source ^(b)	
NGC 1898	0.09 ± 0.07	0.08 ± 0.07	1
NGC 2019	0.04 ± 0.03	0.04 ± 0.03	1
NGC 6287	0.08 ± 0.18	0.08 ± 0.18	2, 3
NGC 6293	0.08 ± 0.18	0.08 ± 0.18	2, 3
NGC 6541	0.00 ± 0.03	0.00 ± 0.03	2, 3
NS97 Halo Stars	0.08 ± 0.03	0.07 ± 0.03	4, 5
NS97 Low- α Stars	0.23 ± 0.11	0.20 ± 0.10	4, 5
Sun	0.22 ± 0.05	0.18 ± 0.01	5, 6
Rup 106	0.39 ± 0.32	0.34 ± 0.31	5, 7
Pal 12	0.38 ± 0.22	0.29 ± 0.18	5, 7
BD+80 245	0.58 ± 0.21	0.47 ± 0.21	5

REFERENCES. — 1 – this study; 2 – Lee & Carney (2002); 3 – Ivans (2005); 4 – Nissen & Schuster (1997); 5 – Ivans et al. (2003); 6 – Anders & Grevesse (1989) with modified iron abundance as discussed in Section 4.1; 7 – Brown et al. (1997);

^(a)Iwamoto et al. (1999).

^(b)Höflich, Khokhlov, & Wheeler (1995); Höflich & Khokhlov (1996); Höflich, Wheeler, & Thielemann (1998); Domínguez, Höflich & Straniero (2001); Höflich et al. 2002.

Two sets of $\langle N_{Ia}/N_{II} \rangle$ are shown, one for each of the two main sources of SNe Ia yields adopted. The SNe II yields are taken from Iwamoto et al. (1999; see references therein), integrated over a Salpeter (1955) initial mass function with SNe II progenitor star masses from 10–50 M_{\odot} . We refer the reader to Ivans et al. (2003) for further details regarding the methods and techniques employed.

Listed for comparison are the $\langle N_{Ia}/N_{II} \rangle$ values derived for Galactic stellar populations of comparable iron abundance, including the sample of low- α stars uncovered in the local solar neighbourhood by NS97, the more metal-poor low- α star BD+80 245, and the low- α clusters, Rup 106 and Pal 12, studied by Brown et al. (1997). The value we derive for $\langle N_{Ia}/N_{II} \rangle$ in the LMC cluster stars is comparable to that of the Galactic halo field stars, and dissimilar to the $\langle N_{Ia}/N_{II} \rangle$ found in the Galactic examples of low- α stars. Thus, the same mixture of Type Ia and Type II ejecta as found in the Milky Way halo low- α stars cannot explain the abundance ratios of the LMC stars. Instead, the α -element abundance ratios of the LMC stars seem to mimic the splintering of the behavior of the α -elements seen in the recent studies of inner halo clusters by Lee & Carney (2002) and Lee et al. (2004) where [Si/Ti] is as high as ~ 0.6 dex for some inner halo GGC stars.

As noted in §1, numerous studies have reported abundance trends with apogalactic distance for stars in our Galaxy. In particular, Lee & Carney and Lee et al. (2004) find abundance trends in α -element ratios that they have interpreted as the result of mass-dependent yields of Type II SNe. In our study, the most interesting abundance ratios also come from the inner LMC clusters, in part because our outer LMC cluster (Hodge 11) is also by far the most metal-poor cluster. Combining our results with those of other clusters which lie at varying distances from the LMC bar (e.g., Hill et al. 2004),

future studies will be able to compare radial trends between the LMC and Milky Way and should prove to be very illuminating.

Different sources of production of the various iron-peak elements could explain the variation we observe in the iron-peak abundance ratios of the LMC cluster stars. Timmes et al. (1995) used the Woosley & Weaver calculations (1995) for Type II SNe and the Thielemann, Nomoto, & Yokoi (1986) calculations for Type Ia SNe to look at the chemical enrichment of the Galaxy over time. They concluded that their model underproduced the solar abundance of V and suggested that there is another source of V, perhaps helium detonations in sub-Chandrasekhar mass models. Nakamura et al. (2001) and Umeda & Nomoto (2002) studied the creation of the iron-peak elements in the extremely energetic class of supernovae known as hypernovae. They found that, since V, along with Cr and Mn, is synthesized in incomplete explosive Si-burning, less energetic explosions would produce less V, Cr and Mn. In the case of the LMC data, we have found subsolar ratios of [V/Fe] and [Mn/Fe] with solar [Cr/Fe]. Thus, we do not favor the hypernovae explanation. Figure 9 compares our [V/Mn] and [V/Cr] values with predictions of the hypernova models of Umeda & Nomoto (2002) and the disagreement is clear, regardless of the energy of the explosion or the mass of the progenitor stars. It could be the case that fewer V-producing Type Ia SNe exploded in the LMC than in the Galaxy at this metallicity. The previous analysis of the α -elements (ignoring Ca and Ti) and iron abundance shows that the LMC clusters have similar $\langle N_{Ia}/N_{II} \rangle$ values to those found in the Galactic halo field stars of comparable metallicity. So simply invoking more SNe Type Ia's at lower metallicities cannot explain the other abundance pattern behaviors with respect to Type Ia iron contributions.

Supporting the argument against low-metallicity SNe Type Ia contributions is the difference in abundance trends between iron-peak elemental ratios. In Galactic field stars, the abundance of [Cu/Fe] as a function of [Fe/H] begins to rise ~ 0.5 dex in [Fe/H] before the [α /Fe] ratio (as a function of [Fe/H]) begins to decrease (where the decrease in [α /Fe] as a function of [Fe/H] is usually taken to be the effect of Fe contributions from Type Ia SNe ejecta). While some Cu can be produced in Type Ia, we favor a metallicity-dependent yield from Type II's as the best explanation of the Galactic data for [Fe/H] < -1 as predicted by the models of Woosley & Weaver (1995) and in Timmes et al. (1995). The abundances of the LMC cluster and ω Cen stars (see Figure 7) do not appear to require much contribution by Type Ia supernovae. Since the production of Cu in the LMC matches the production of Fe, we conclude that there is a minimum [Cu/Fe] produced in another source, possibly the result of massive star contributions. The lack of any trend in [Cu/Fe] with metallicity in the LMC and ω Cen could be due to continued contributions from metal-poor SNII or the lack of contributions from Type Ia SNe. For the LMC clusters, either of these ideas is in accord with the old ages previously measured. Thus, these results support the idea that the main *s*-process is not likely to be a substantial contributor to Cu production (Matteucci et al. 1993). However, in the case of the LMC, it may have experienced a history similar to that of the

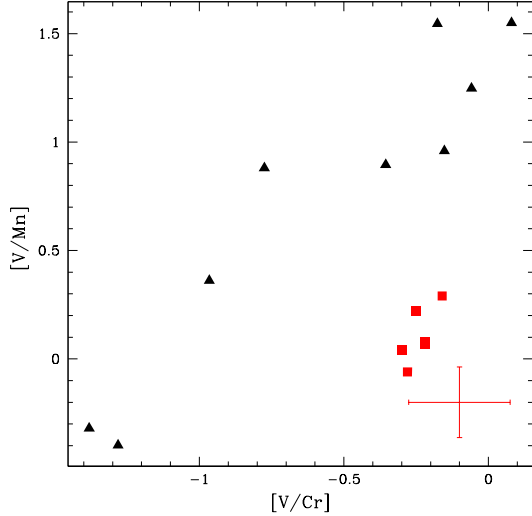


FIG. 9.— Comparison of the $[V/Cr]$ vs $[V/Mn]$ for LMC stars in our sample (filled squares) with the Umeda & Nomoto (2002) predictions for the yields of hypernovae (filled triangles) with different progenitor masses ($13\text{--}30M_{\odot}$) and explosion energies ($1\text{--}50 \times 10^{51}$ ergs). These models were made for zero-metallicity stars, but that should not affect the results here, since the most important variables in the iron-peak ratios are the explosion energy and the mass cut. A typical errorbar is shown for our derived abundances. The Umeda & Nomoto hypernovae yields do not explain the abundances we observe in the LMC cluster stars.

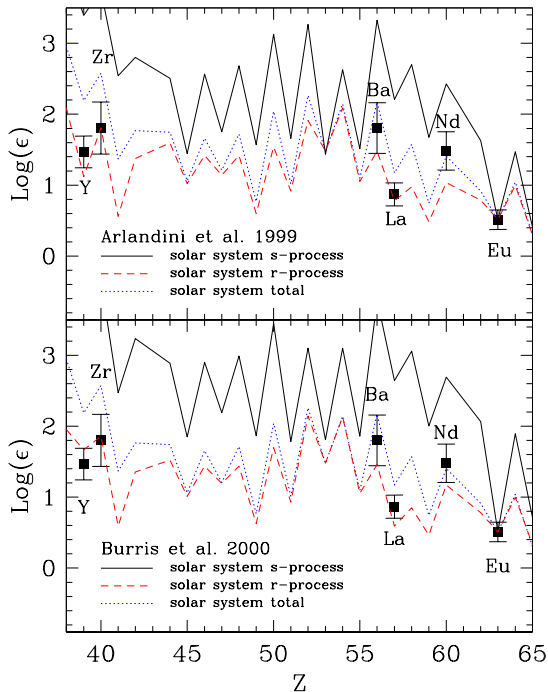


FIG. 10.— Comparison of the average $\log \epsilon$ of four LMC stars with the solar system r -process, s -process and total fractions from Arlandini et al. (1999) (top) and Burris et al. (2000) (bottom). Because we are comparing results derived for stars with different metallicities, we first normalized all the $\log \epsilon(\text{Eu})$ values to those of NGC 1898#1. Next, all the abundances were averaged. The solar values were then adjusted to match this normalized, averaged Eu value. The agreement between the data and the solar system r -process pattern, especially for Eu and La, shows that there is little, if any, contribution of the s -process to the heavy elements abundances in the LMC clusters.

Sgr dSph (see Figure 7). More relatively metal-rich LMC stars need to be observed in order to discern whether or not a rise in the Cu abundance exists with respect to the Fe abundance.

We explored the origin of the neutron-capture elements in our clusters by comparing the r -process and s -process contributions to the solar system abundances with the observed LMC abundances (Figure 10). Our La and Eu abundances are the most reliable, since their lines are mostly on the linear part of of the curve of growth and both HFS and isotopic splitting are fully taken into account. Viewing the fit to La and Eu (and the other neutron-capture elements), we favor an r -process contribution with, at most, a 20% contribution from the s -process to improve the agreement with Ba, Nd, and Y. Thus, the LMC clusters have little, if any, contribution from the main s -process, while the more metal-rich ω Cen stars are s -process-rich (e.g., Smith et al. 2000), yet both share the groups of stars low with $[\text{Cu}/\text{Fe}]$ ratios.

The low s -process abundances are a natural consequence of the LMC clusters being among the first objects formed in the Clouds, before much chemical evolution took place, and before AGB stars had time to evolve and contribute their yields to the interstellar mix. We have argued in this section that the addition of iron from Type Ia ejecta is not the solution to the abundance ratios that we see, though the lack of Type Ia contributions may be part of the reason for the low $[\text{Cu}/\text{Fe}]$ and $[\text{V}/\text{Fe}]$.

6. SUMMARY AND CONCLUSIONS

Employing a linelist of >300 lines with laboratory-based gf -values, we have derived elemental abundances for the α -, iron-peak, and neutron-capture element groups of ten giant stars in four old globular clusters of the LMC. In deriving the abundances of Sc, V, Mn, Co, Cu, Ba, La, and Eu, we took into account HFS in all of the lines employed. Extensive numerical experiments were performed to elucidate the effects of differing choices of gf -values, stellar atmospheres, and stellar parameters on the abundances we derived.

While we find that many abundance similarities exist between the globular cluster stars in the LMC and our Galaxy (e.g., the ratios of $[\text{O}/\text{Fe}]$, $[\text{Na}/\text{Fe}]$, $[\text{Al}/\text{Fe}]$, $[\text{Mg}/\text{Fe}]$, and $[\text{Si}/\text{Fe}]$), the same is not true of all of the elements we studied. In particular, we find differences *within both* the α -element *and* iron-group abundances. We find lower-than-MWG-average values, and indeed, in some cases, clearly sub-solar values of $[\text{Ca}/\text{Fe}]$, $[\text{Ti}/\text{Fe}]$, $[\text{V}/\text{Fe}]$, $[\text{Ni}/\text{Fe}]$. The LMC cluster giant star abundances of $[\text{Co}/\text{Fe}]$, $[\text{Cr}/\text{Fe}]$ and $[\text{Mn}/\text{Fe}]$ may indicate additional offsets. However, the available literature on the Galactic abundances of this trio of iron-peak elements is sparse (in one or the other of the globular cluster or field star populations) and further data are required to determine with greater certainty whether the differences in the abundances derived for the different groups are significant.

In the case of another iron-peak element, the behavior of $[\text{Cu}/\text{Fe}]$ in our LMC clusters with respect to $[\text{Fe}/\text{H}]$ appears to be constant with a value of ~ -0.8 . While this is in marked contrast to the abundances observed in other MWG halo field and cluster stars, it does resemble the trend observed in ω Cen. More relatively metal-rich LMC stars need to be observed in order to discern whether or not a rise in the Cu abundance exists with respect to the

Fe abundance

With regards to the neutron-capture elemental abundance ratios of [Y/Fe], [Ba/Fe], and [Eu/Fe], we find the LMC star results to be similar to the MWG-average values. We compared the abundances derived for NGC1898 and NGC2019 against predictions of the scaled solar system contributions of the r - and s -process by Arlandini et al. (1999) and Burris et al. (2000). We find that the abundances of neutron-capture elements Y, Zr, Ba, La, Nd, and Eu can largely be accounted for by the r -process, with, at most, a 20% contribution from the s -process to improve the agreement with Y, Ba, and Nd.

The abundance ratio distributions observed in red giant stars in the LMC globular clusters are markedly different from those found in the GGC red giants, the halo field red giants, and the red giant stars of the dSph systems. Since the α elements in the LMC clusters are not universally suppressed, and the ages of these clusters are old, we do not favor contributions by Type Ia SNe, but rather a unique star formation history that produced smaller amounts of Ca, Ti, V, Ni and Cu than in the Milky Way. Possible explanations include a bias in the mass function of SNe that either exploded or whose ejecta were retained, or stars in the LMC being formed from material resulting from contributions by lower metallic-

ity SNe than in our Galaxy. The cause of the low [Y/Fe] values seen in the stars of dSph systems does not operate in the LMC clusters, and marks another difference, in addition to the [Mg/Fe] and [Si/Fe] values, between the LMC and the dSph systems. There do not appear to be universal trends among the satellite galaxies of the Galaxy. We conclude that many of the abundances in the LMC globular clusters we observed are distinct from those observed in the Milky Way, and these differences are intrinsic to the stars in those systems.

This research has made use of NASA’s Astrophysics Data System Bibliographic Services; the SIMBAD database, operated at CDS, Strasbourg, France; and the NASA/IPAC Extragalactic Database which is operated by the Jet Propulsion Laboratory, California Inst. of Technology, under contract with NASA. III is pleased to acknowledge research support from NASA through Hubble Fellowship grant HST-HF-01151.01-A from the Space Telescope Science Inst., operated by AURA, under NASA contract NAS5-26555. Mike Bolte, Jon Fulbright, Jim Hesser, Bob Kraft, and Andy McWilliam are warmly thanked for their helpful and illuminating discussions as well as for readily supplying data in electronic form.

APPENDIX

ERROR ANALYSIS

For all elemental abundances derived in this study, the two major sources of uncertainty are the EW measurements and the choice of model atmospheres, both of which overwhelm those from the $\log gf$ -values. As discussed in Section 3.1, the EW uncertainties can be accounted for by the line-to-line scatter. For a given elemental abundance, if a smaller than expected value of dispersion resulted from the use of a small number of lines (i.e., where the standard deviation of the sample was < 0.05 dex), we derived a more accurate value by calculating the expected uncertainty in the EW for each line, and adopting the average uncertainty produced. The model atmosphere parameters are not independent and are correlated in several different ways. We follow the basic method outlined by McWilliam et al. (1995) and adapted by Johnson (2002):

$$\begin{aligned} \sigma_{\log \epsilon}^2 = & \sigma_{EW}^2 + \left(\frac{\partial \log \epsilon}{\partial T} \right)^2 \sigma_T^2 + \left(\frac{\partial \log \epsilon}{\partial \log g} \right)^2 \sigma_{\log g}^2 + \left(\frac{\partial \log \epsilon}{\partial [m/H]} \right)^2 \sigma_{[m/H]}^2 + \left(\frac{\partial \log \epsilon}{\partial \xi} \right)^2 \sigma_{\xi}^2 \\ & + 2 \left[\left(\frac{\partial \log \epsilon}{\partial T} \right) \left(\frac{\partial \log \epsilon}{\partial \log g} \right) \sigma_{T \log g} + \left(\frac{\partial \log \epsilon}{\partial [m/H]} \right) \left(\frac{\partial \log \epsilon}{\partial \log g} \right) \sigma_{\log g [m/H]} \right. \\ & \left. + \left(\frac{\partial \log \epsilon}{\partial [m/H]} \right) \left(\frac{\partial \log \epsilon}{\partial T} \right) \sigma_{T [m/H]} \right] + \left(\frac{\partial \log \epsilon}{\partial \xi} \right) \left(\frac{\partial \log \epsilon}{\partial [m/H]} \right) \sigma_{\xi [m/H]}, \end{aligned}$$

where $\sigma_{T \log g}$, for example, is defined as

$$\sigma_{T \log g} = \frac{1}{N} \sum_{i=1}^N (T_i - \bar{T}) (\log g_i - \overline{\log g}). \quad (\text{A1})$$

The uncertainties in T_{eff} and $\log g$ are clearly correlated, not only due to the explicit $\log g$ - T_{eff} dependence, but also due to the dependence of the bolometric correction on the temperature. Equation 1 reveals the other sources of random error in $\log g$. We adopted uncertainties of 0.1 mag in V magnitude, to account for possible systematics unaccounted for in the quoted random uncertainties of 0.05 mag. We estimate the uncertainty in the apparent distance modulus as 0.2 mag. Finally, we adopt an uncertainty of 0.05 solar masses for stellar mass. Below, we discuss the effect of a possible systematic difference of 0.25 solar masses, as a result of assuming an RGB mass for a star which has actually undergone mass loss.

Alonso et al. (1999) give separate formulae for the bolometric correction depending on the temperature. Thus, $\sigma_{T \log g}$ was not determined analytically. Instead, we devised the following method to determine the uncertainty in $\log g$ and the covariance between T_{eff} and $\log g$. We ran 1000 test cases with errors added to T_{eff} , V magnitude, $(m-M)_V$, and BC with their appropriate σ s. A $\log g$ was then calculated. The set of $\log g$ and T_{eff} allowed us to find $\sigma_{T \log g}$.

We used Fe II to determine the model metallicity ($[m/H]$), which is very sensitive to $\log g$ and T_{eff} . There is an insufficiently strong correlation between excitation potential and EW to produce a noticeable correlation in the

TABLE B18
PHOTOMETRIC & SPECTROSCOPIC TEMPERATURES

Star	V	V-I	V-I ₀	m-M _V	T _{eff} (Alonso)	T _{eff} (Houdashelt)	T _{eff} (Spec)
NGC 1898#1	16.588	1.614	1.522	18.69	3923	4101	4050
NGC 1898#2	16.464	1.654	1.562	18.69	3889	4084	4000
NGC 2005#1	16.374	1.700	1.568	18.69	3883	4091	4050
NGC 2005#2	16.924	1.561	1.429	18.69	4026	4161	4350
NGC 2005#3	16.834	1.646	1.514	18.69	3931	4098	4250
NGC 2019#1	16.564	1.306	1.227	18.62	4306	4415	4250
NGC 2019#2	16.465	1.582	1.503	18.62	3943	4124	4050
NGC 2019#3	16.248	1.720	1.641	18.62	3821	4064	3950

uncertainties of T_{eff} and ξ. Our uncertainty in ξ is 0.3 km/s. While our Fe II lines are fairly weak, there is a correlation between the value for ξ and [m/H]. Since there is a large uncertainty in Fe II due to EW uncertainties, we performed a similar calculation to our σ_{Tlog g} calculation to derive σ_{ξ[m/H]}, as well as σ_{log g[m/H]} and σ_{T[m/H]}. The uncertainty in the abundance ratios is not necessarily equal to adding the uncertainties in [X/H] in quadrature. Instead we use equation A19 from McWilliam et al. (1995):

$$\sigma(A/B)^2 = \sigma(A)^2 + \sigma(B)^2 - 2\sigma_{A,B}. \quad (\text{A2})$$

where the covariance σ_{A,B} has been modified from eq. A20 in McWilliam et al. (1995) to take into account the uncertainty in [m/H]:

$$\begin{aligned} \sigma_{A,B} = & \left(\frac{\partial \log \epsilon_A}{\partial T} \right) \left(\frac{\partial \log \epsilon_B}{\partial T} \right) \sigma_{\log g}^2 + \left(\frac{\partial \log \epsilon_A}{\partial \log g} \right)^2 \left(\frac{\partial \log \epsilon_B}{\partial \log g} \right)^2 \sigma_{\log g}^2 \\ & + \left(\frac{\partial \log \epsilon_A}{\partial [m/H]} \right)^2 \left(\frac{\partial \log \epsilon_B}{\partial [m/H]} \right)^2 \sigma_{[m/H]}^2 + \left(\frac{\partial \log \epsilon_A}{\partial \xi} \right)^2 \left(\frac{\partial \log \epsilon_B}{\partial \xi} \right)^2 \sigma_{\xi}^2 \\ & + \left[\left(\frac{\partial \log \epsilon_A}{\partial T} \right) \left(\frac{\partial \log \epsilon_B}{\partial \log g} \right) + \left(\frac{\partial \log \epsilon_A}{\partial \log g} \right) \left(\frac{\partial \log \epsilon_B}{\partial T} \right) \right] \sigma_{T \log g} \\ & + \left[\left(\frac{\partial \log \epsilon_A}{\partial \log g} \right) \left(\frac{\partial \log \epsilon_B}{\partial [m/H]} \right) + \left(\frac{\partial \log \epsilon_A}{\partial \log g} \right) \left(\frac{\partial \log \epsilon_B}{\partial [m/H]} \right) \right] \sigma_{\log g [m/H]} \\ & + \left[\left(\frac{\partial \log \epsilon_A}{\partial T} \right) \left(\frac{\partial \log \epsilon_B}{\partial [m/H]} \right) + \left(\frac{\partial \log \epsilon_A}{\partial [m/H]} \right) \left(\frac{\partial \log \epsilon_B}{\partial T} \right) \right] \sigma_{T [m/H]} \\ & + \left[\left(\frac{\partial \log \epsilon_A}{\partial \xi} \right) \left(\frac{\partial \log \epsilon_B}{\partial [m/H]} \right) + \left(\frac{\partial \log \epsilon_A}{\partial [m/H]} \right) \left(\frac{\partial \log \epsilon_B}{\partial \xi} \right) \right] \sigma_{T \log g} \end{aligned} \quad (\text{A3})$$

DISCUSSION OF MODEL ATMOSPHERE PARAMETERS

Our choice of model atmosphere parameters was a critical part of our abundance calculations. For most elements, we measure a sufficient number of lines with reliable *gf*-values to make the uncertainty in the effective temperatures the dominant source of uncertainty. In this appendix, we discuss more fully the changes in abundance ratios that occur when different atmosphere parameters are adopted.

Effective Temperatures

T_{eff} can be derived in a number of ways. We limit our discussions here to those derived either photometrically, using colours (photometric T_{eff}), or spectroscopically, using the abundance derived for Fe I lines with different lower excitation potentials (excitation T_{eff}). In the main body of this paper, we adopted the latter method also used by Shetrone et al. (2003) in their studies of giants in dSphs, and by the bulk of the studies done by the Lick-Texas group in their analyses of GGC stars.

In their re-evaluation of the abundance scale of globular clusters using Fe II, Fe-KI03 employed photometric T_{eff} values because of concerns with the possibility of overionization of Fe I. For the RGB stars included in their study, they concluded that T_{eff} derived spectroscopically and photometrically were similar, but because of the degeneracy between T_{eff} and log *g* on the RGB, spectroscopic temperatures tended to have greater uncertainty. We possess photometry for most of the stars in our sample and can compare the T_{eff} derived by different means. To correct for reddening, and we use the adopted values E(B-V) from O98 for NGC 2019, NGC 1898 and NGC 2005 and Walker (1993) for Hodge 11, combined with the E(B-V)/E(V-I) value from Sarajedini (1994). We used the Cousins/Johnson color transformations of Bessell (1979). Table 18 shows our calculated T_{eff} for the Alonso et al. (1999) calibration and the Houdashelt, Sweigart, & Bell (2000) calibration. We used the Ramírez and Meléndez (2005) color-T_{eff} calibration

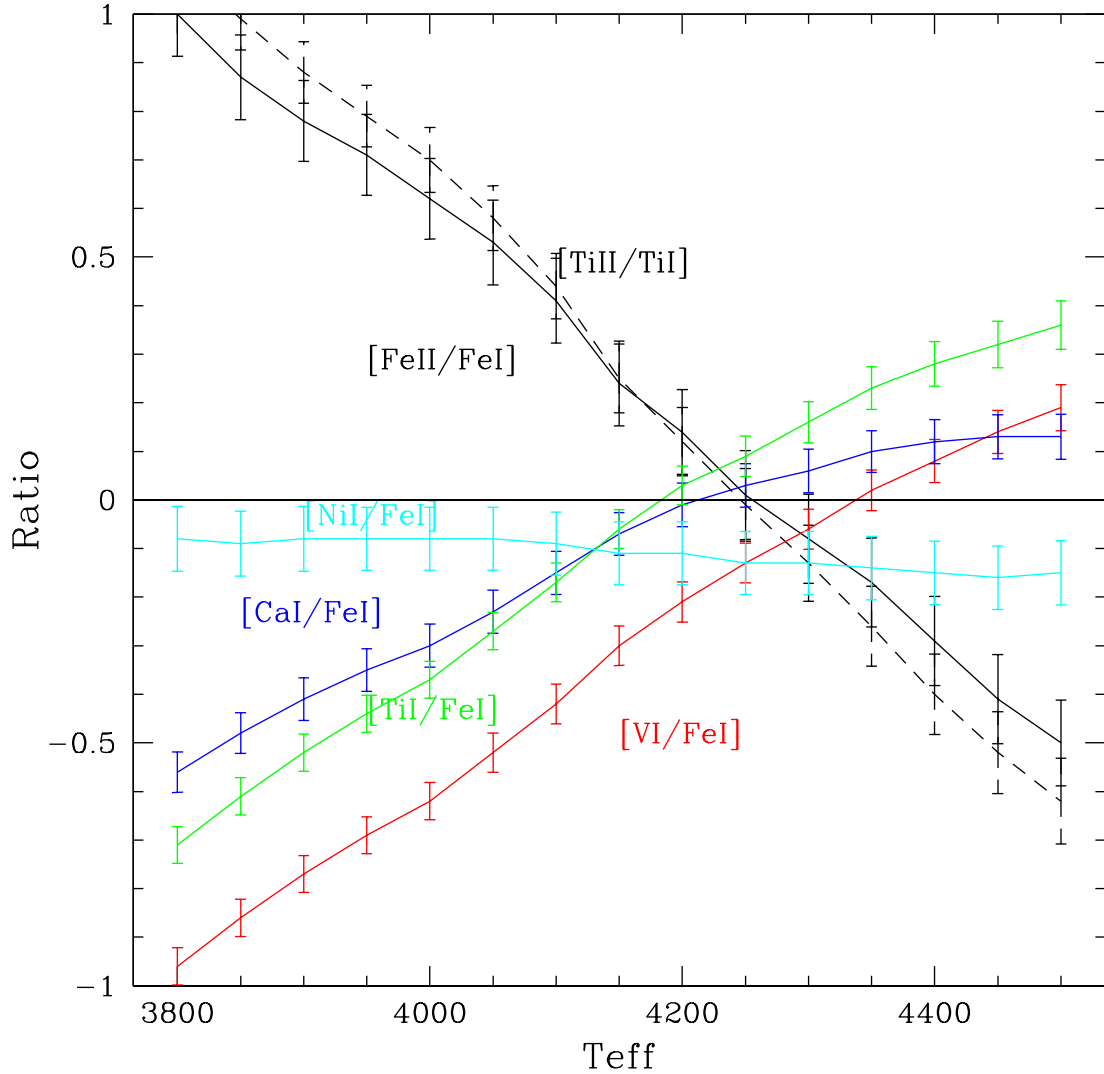


FIG. B1.— Effect on abundance ratios of changing atmospheric parameters for NGC 1898#1. The T_{eff} of the model is shown on the horizontal axis, but the $\log g$ and $[m/H]$ are changing as well (see § B1). The largest impact on the abundance ratios are due to changes in T_{eff} (see Figure 2). Increasing the T_{eff} improves the agreement between neutral and ionized species and raises $[V/Fe]$ and $[Ti/Fe]$ closer to solar values. However, we cannot find a T_{eff} that simultaneously makes $[Ca/Fe]$ and $[Ti/Fe] \sim 0.3$ dex and $[V/Fe]$ and $[Ni/Fe] \sim 0$ (MWG-average values for unevolved dwarf stars of comparable metallicity). The temperatures closest to realizing this are unrealistically too hot for stars on the red giant branch.

on stars that were blue enough to be included in their system, and found T_{eff} s within the range covered by Alonso et al. and Houdashelt et al.

It is apparent that for the inner LMC clusters NGC 1898, NGC 2005 and NGC 2019, the T_{eff} predictions from the color-temperature calibrations are a poor match to those we derive spectroscopically. A change of about 0.15 mag in the $V - I$ color due to either uncertainties in reddening or in photometry would reconcile the spectroscopic and Alonso photometric T_{eff} values. These stars are saturated in the long exposures of LMC-O98, and because of charge-transfer efficiency effects, the length of exposure has an impact on the photometry. LMC-O98 added a magnitude-dependent correction to put the short exposures on the same system as the long exposures. Unfortunately, these clusters have not been successfully studied from the ground, therefore an independent source of photometry does not exist to check the accuracy of the *HST* results.

Could the non-standard abundance ratios we observe be eliminated by any logical choice of T_{eff} ? To check this possibility, we performed the following test. We interpolated a series of Kurucz model atmospheres with T_{eff} from 3800K to 4500K, $\log g$ derived from Equation 1 for the star NGC 1898#1, and $[m/H]$ derived from Fe II lines. In Figure B1, we plot several important abundance ratios as a function of the T_{eff} of the model atmospheres. Many abundance ratios are very dependent to the adopted T_{eff} , and hotter models for NGC 1898#1 often produced, for some elements, better agreement with ratios derived in the GGCs. However, other than a desire for standard Galactic GC abundance ratios, there is no reason to adopt these temperatures and several reasons to avoid this course.

First, the spectroscopic and photometric T_{eff} values are in stark disagreement with the “chemical temperatures” derived from forcing $[V/\text{Fe}] \sim 0$. The reddening of NGC 1898 would have to be 0.32 mag redder in $E(B-V)$ to make the stars sufficiently blue to have the photometric T_{eff} as high as the chemical T_{eff} . Second, when we compare the chemical T_{eff} to the T_{eff} derived in other studies for stars in clusters with similar metallicities, we find the chemical T_{eff} too high for stars at the tip of the red giant branch of a globular cluster. Our derived $[\text{Fe}/\text{H}]$ and our adopted effective temperature are correlated, so raising T_{eff} decreases the abundance from Fe II lines. However, the metallicity implied by Fe II does not decrease quickly enough with increasing temperature to reconcile the temperatures. We conclude that (i) adopting the Alonso photometric T_{eff} would make the abundance ratios such as $[\text{Ca}/\text{Fe}]$, $[\text{Ti}/\text{Fe}]$ and $[\text{Sc}/\text{Fe}]$, even more distinct from the standard GGC ratios and (ii) adopting a chemical T_{eff} that force abundance ratios close to those observed in standard GGCs would require unacceptable reddening and temperatures for the cluster stars.

Gravities

In the analysis presented in the main body of the paper, we employed evolutionary $\log g$ values. Many recent studies also use this technique (see e.g., Cohen et al. 2001; M5-I01). It has the advantage that when choosing the gravity, overionization has no effect and the adopted metallicity, only a small effect.

A comparison with the Bergbusch and Vandenberg isochrones reveals that our choice of atmospheric parameters for NGC 1898, and NGC 2019 cause the stars to occupy a hotter, higher luminosity region than an isochrone with $Z = [\text{Fe II}/\text{H}]$ (Figure 2B). A decrease in the T_{eff} we chose could reconcile the evolutionary and isochronic $\log g$ values. If we changed $\log g$ by changing the distance or the bolometric correction, we need to make a larger correction than shown in Figure A2. Because the derived Fe II is very sensitive to the adopted $\log g$, an increase in $\log g$ would force the adoption of a higher Z isochrone. For the parameters used here, this process converges with an increase in $\log g$ of 0.3 dex and an increase in $[\text{Fe II}/\text{H}]$ of 0.15 dex.

We also investigated the consequence of assuming too large a mass for these tip stars. If instead of having a mass of $0.85 M_{\odot}$, these stars may have undergone sufficient mass loss to have a typical mass of an HB star ($0.6 M_{\odot}$). Equation 1 shows that the calculated $\log g$ would decrease by 0.15 dex. However, for most cases, the change in the derived abundances is <0.1 dex. As shown in Figure 2, these changes are smaller than those due to temperature uncertainties.

The discrepancy between the abundance from Fe I and Fe II lines could be reduced by adopting a lower $\log g$. However, even by reducing the $\log g$ to 0, the limit of the Kurucz grid, we were still ~ 0.1 dex from ionization equilibrium for several stars. Eq. 1 shows that decreasing $\log g$ by 0.7-1.0 dex would result in an unacceptably large increase in the distance modulus to the LMC of 1.75-2.5 mag. Thus, the evolutionary $\log g$ values, along with the previously published distance estimates, are the most correct $\log g$ values to employ here.

Choice of grid of model atmospheres

We interpolated model atmospheres using the standard grid of Kurucz models with overshooting (Kurucz 1992, 1993). Other possible choices include Kurucz models without overshooting (Castelli, Gratton, & Kurucz 1997), Kurucz models without overshooting, but with new opacity distribution function sampling and enhancements in the α -elements (Castelli & Kurucz 2003), an early version of MARCS (Bell et al. 1976) models, and the updated MARCS spherically geometric models (Gustafsson et al. 2002)⁸. Table 19 summarizes the effect on the abundance ratios of star NGC 2019#2 for those model atmospheres in the above order. The second column displays the results found in our study and the remaining columns display the difference in the abundance derived employing an alternate model in the sense of $\Delta \equiv (\text{alternative model results}) - (\text{this study})$.

We find a similar result to M4-I99 when comparing the effect of the different models, namely that the original MARCS models gave similar answers to Kurucz models that were 50K hotter. In general, the choice of the grid of model atmospheres is a much smaller source of uncertainty than the choice of T_{eff} . However, we note the significant revision one would find if the spherically geometric models were employed in place of plane-parallel models used in this study (and in all of the abundance studies with which we have compared our results against): the difference between the derived abundances of Fe I and Fe II increases from 0.5 to 0.7 dex.

Oscillator Strengths

In order to investigate the difference made by using our linelist vs. those of other selected studies, we performed the following experiment. We redid the analysis for star NGC 2019#2 using the line lists of M5-I01 and Shetrone et al. (2001) and our equivalent widths and HFS constants. As seen in Table 3B, for many elements the results do not change by more than 0.05 dex. In the cases with larger deviations, this is mainly due to the small number of lines and the uncertainties in the EWs, rather than large changes in the gf -values.

Summary

A variety of methods can be used to determine the model atmosphere parameters of cool giant stars. In the ideal situation, all of the methods would provide consistent answers. However, this is seldom the case. In this appendix, we have investigated the effect of choices in temperature (photometric vs. spectroscopic), reddening and distance modulus, $\log g$ and evolutionary state, model atmosphere code, and adopted atomic parameters. In no instance do any of these experiments force us to significantly revise the abundance ratios derived in this study. Instead, we conclude that

⁸ Grids of the new MARCS model atmospheres can be downloaded from <http://www.marcs.astro.uu.se>.

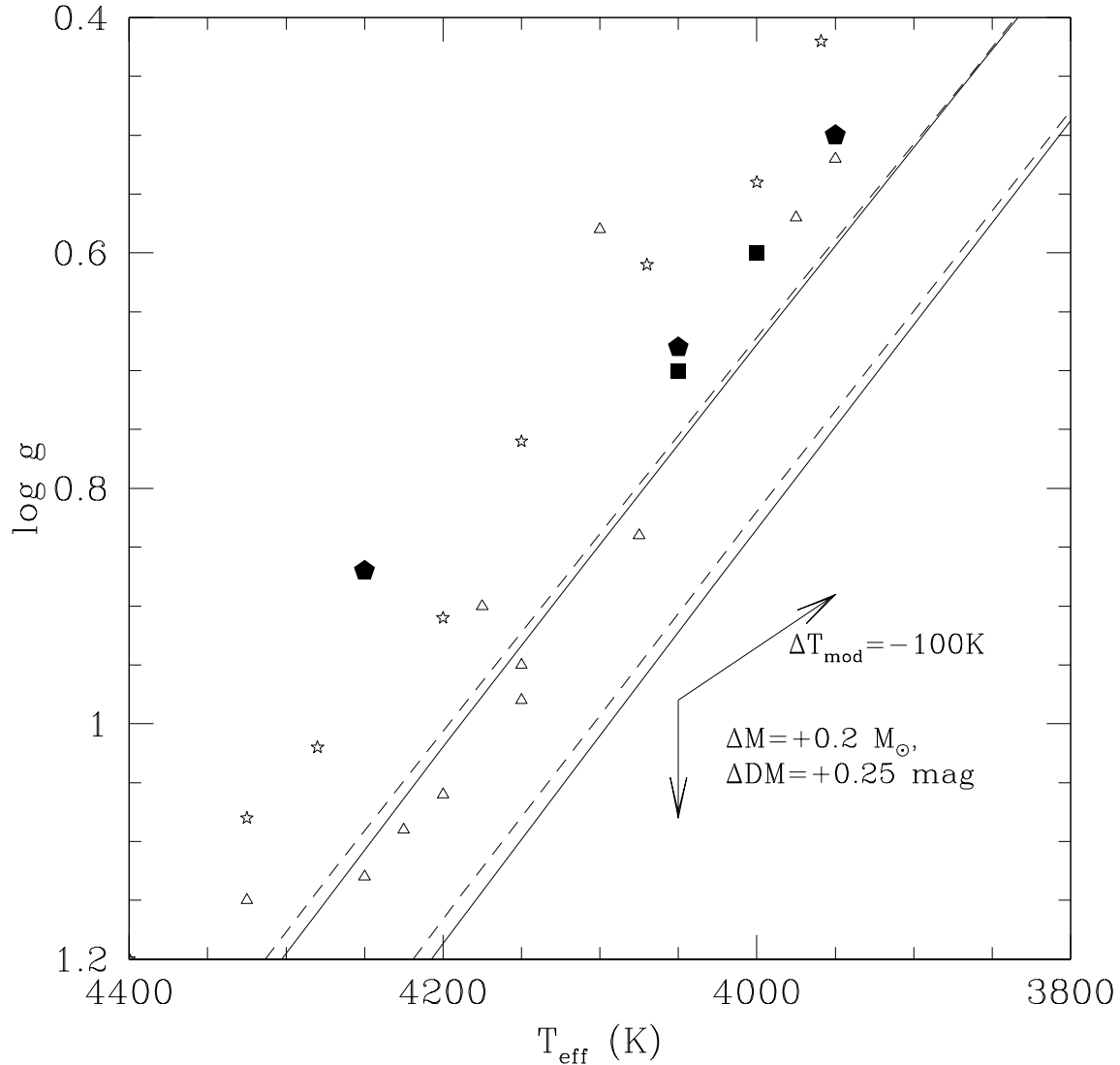


FIG. B2.— Comparison of our adopted $\log g$ values with the Bergbusch & Vandenberg (1992) isochrones for stars in two clusters with similar metallicities: NGC 1898 and NGC 2019 (filled symbols). The $Z = 0.0017$ and 0.001 ($[m/H] = -1.03$ and -1.26 , respectively) isochrones of 8 Gyr (dashed) and 12 Gyr (solid) are plotted. The more metal-rich isochrones lie to the right. Stars from M4-I99 (open triangles) ($[Fe/H] = -1.15$) and M5-I01 (open stars) ($[Fe/H] = -1.24$) are also shown. The metallicities derived from Fe II lines for the LMC clusters make them slightly more metal-rich than M4 or M5, so their points should lie either to the right or down from the other clusters. The arrows indicate the magnitude of the shift in the Kiel diagram if the temperature of the model (which in turn affects the $\log g$ as shown in Eq. 1), the mass of the star, or the distance modulus were changed by the indicated amount.

many of the abundances in the LMC globular cluster stars are distinct from those observed in GGC stars of similar metallicities and these differences are intrinsic to the stars in those systems, not induced by the method of analysis.

REFERENCES

- Alonso, A., Arribas, S., & Martínez-Roger, C. 1999, *A&AS*, 140, 261
- Anders, E. & Grevesse, N. 1989, *Geochim. Cosmochim. Acta*, 53, 197
- Aoki, W., Ryan, S. G., Norris, J. E., Beers, T. C., Ando, H., Iwamoto, N., Kajino, T., Mathews, G. J., & Fujimoto, M. Y. 2001, *ApJ*, 561, 346
- Arlandini, C., Käppeler, F., Wisshak, K., Gallino, R., Lugaro, M., Busso, M., & Straniero, O. 1999, *ApJ*, 525, 886
- Arnett, D. 1971, *ApJ*, 166, 153
- Bai, G. S., Zhao, G., Chen, Y. Q., Shi, J. R., Klochkova, V. G., Panchuk, V. E., Qiu, H. M., & Zhang, H. W. 2004, *A&A*, 425, 671
- Bard, A. & Kock, M. 1994, *A&A*, 282, 1014
- Bard, A., Kock, A., & Kock, M. 1991, *A&A*, 248, 315
- Baumüller, D., Butler, K., & Gehren, T. 1998, *A&A*, 338, 637
- Bell, R. A., Eriksson, K., Gustafsson, B., & Nordlund, A. 1976, *A&AS*, 23, 37
- Bellazzini, M., Ferraro, F. R., & Ibata R. 2003, *AJ*, 125, 188
- Bessell, M. S. 1979, *PASP*, 91, 589
- Bergbusch, P. A., & Vandenberg, D. A. 1992, *ApJS*, 81, 163
- Bernstein, R., Shtetman, S. A., Gunnels, S. M., Mochnecki, S., & Athey, A. E. 2003, *Proceedings of the SPIE*, 4841, 1694
- Blackwell, D. E., Booth, A. J., Haddock, D. J., Petford, A. D., & Leggett, S. K. 1986, *MNRAS*, 220, 549
- Blackwell, D. E., Booth, A. J., Menon, S. L. R., & Petford, A. D. 1986, *MNRAS*, 220, 289
- Blackwell, D. E., Menon, S. L. R., & Petford, A. D. 1983, *MNRAS*, 204, 883
- Blackwell, D. E., Menon, S. L. R., & Petford, A. D. 1984, *MNRAS*, 207, 533

TABLE B19
NGC 2019#2 Δ ABUNDANCES DUE TO MODEL ATMOSPHERE GRID CHOICES

Species	Kurucz over	Δ Kurucz nover	Δ Kurucz α	Δ MARCS old	Δ MARCS new
O I	7.93	0.00	0.08	-0.03	0.13
Na I	4.73	-0.01	-0.01	0.02	-0.09
Mg I	6.60	0.00	0.05	-0.02	-0.01
Ca I	4.97	-0.01	0.06	-0.06	-0.08
Sc II	1.87	0.02	0.11	-0.05	0.16
Ti I	3.57	-0.01	0.05	0.08	-0.08
Ti II	4.16	0.00	0.10	-0.05	0.16
V I	2.24	-0.01	0.06	0.09	-0.06
Cr I	4.21	-0.01	0.04	0.04	-0.07
Mn I	3.59	-0.01	0.04	0.02	0.00
Fe I	6.10	0.00	0.07	-0.02	0.07
Fe II	6.58	0.01	0.15	-0.10	0.28
Co I	3.48	0.00	0.06	-0.02	0.07
Ni I	4.67	0.01	0.09	-0.02	0.11
Cu I	2.06	0.00	0.07	-0.02	0.08
Y II	0.73	0.00	0.09	-0.04	0.13
Zr I	1.32	-0.02	0.09	0.13	-0.05
Ba II	0.88	0.01	0.15	0.02	0.16
La II	0.15	0.00	0.10	-0.04	0.16
Nd II	0.59	0.00	0.10	-0.03	0.14
Eu II	-0.06	0.00	0.10	-0.06	0.18

^a $\Delta \equiv$ (alternative model results) - (this study).

TABLE B20
EFFECT OF LINELISTS ON ABUNDANCES OF NGC 2019#2

Species	This Study	# of lines	M5-I01	# of lines	dSph-S01	# of lines
O I	7.93	1	7.93	1
Na I	4.73	2	4.73	2
Mg I	6.60	2	6.60	2
Al I	5.07	1	5.29	1
Ca I	4.97	15	5.03	3	5.07	3
Ti I	3.57	27	3.61	5
Ti II	4.16	6	4.33	1
V I	2.24	14	2.12	1	2.27	4
Fe I	6.10	127	6.11	21	6.11	27
Fe II	6.58	4	6.39	3	6.49	3
Ni I	4.67	18	4.74	2
Y II	0.73	5	0.97	1
Nd II	0.67	4	0.54	1
Eu II	-0.06	1	-0.14	1	-0.14	1
Sc II	1.87	4	1.97	2
Mn I	3.59	3	3.59	3
Co I	3.48	5	3.47	1
La II	0.15	2	0.38	1
Ba II	0.88	2	0.88	2

Blackwell, D. E., Menon, S. L. R., Petford, A. D., & Shallis, M. J. 1982b, MNRAS, 204, 883
 Blackwell, D. E., Petford, A. D., Shallis, M. J., & Leggett, S. K. 1982a, MNRAS, 199, 21
 Blackwell, D. E., Petford, A. D., Shallis, M. J., & Simmons, G. J. 1980, MNRAS, 191, 445
 Blackwell, D. E., Petford, A. D., Shallis, M. J., & Simmons, G. J. 1982c, MNRAS, 199, 43
 Blackwell, D. E., Petford, A. D., & Simmons, G. J. 1982, MNRAS, 201, 595
 Blackwell, D. E., Ibbetson, P. A., Petford, A. D., & Shallis, M. J. 1979, MNRAS, 186, 633
 Blackwell, D. E., Petford, A. D., & Shallis, M. J. 1979, MNRAS, 186, 657
 Booth, A. J., Shallis, M. J., & Wells, M. 1983, MNRAS, 205, 191

Brocato, E., Castellani, V., Ferraro, F. R., Piersimoni, A. M., & Testa, V. 1996, MNRAS, 282, 614
 Brown, J. A., & Wallerstein, G. 1992, AJ, 104, 1818
 Brown, J. A., Wallerstein, G. & Gonzalez, G. 1999, AJ, 118, 1245
 Brown, J. A., Wallerstein, G. & Zucker, D. 1997, AJ, 114, 180
 Buonanno, R., Buscema, G., Fusi Pecci, F., Richer, H. B., & Fahlman, G. G. 1990, AJ, 100, 1811
 Buonanno, R., Corsi, C. E., Fusi Pecci, F., Fahlman, G., & Richer, H. B. 1994, ApJ, 430, L121
 Burris, D.L., Pilachowski, C.A., Armandroff, T.E., Sneden, C., Cowan, J. J. & Roe, H. 2000, ApJ, 544, 302
 Busso, M., Gallino, R., & Wasserburg, G., J. 1999, ARA&A, 37, 239
 Cardon, B. L., Smith, P. L., Scalo, J. M., Testerman, L., & Whaling, W. 1982, ApJ, 260, 395
 Carretta, E., Bragaglia, A., & Cacciari, C. 2004, ApJ, 610, L25

- Carretta, E., Gratton, R. G., Bragaglia, A., Bonifacio, P., & Pasquini, L. 2004, *A&A*, 416, 925
- Castelli, F., & Kurucz, R. L. 2003, in *Modelling of Stellar Atmospheres*, (ed) N. E. Piskunov, W. W. Weiss, D. F. Gray, ASP, 210, 20
- Childs, W. J., Poulsen, O., Goodman, L. S., & Crosswhite, H. 1979, *Phys. Rev. A*, 19, 168
- Cochrane, E. C. A., Benton, D. M., Forest, D. H., & Griffith, J. A. R. 1998, *J. Phys. B*, 31, 2203
- Cohen, J. G. 2004, *AJ*, 127, 1545
- Cohen, J. G., Gratton, R. G., Behr, B. B., & Carretta, E. 1999, *ApJ*, 523, 739
- Cottrell, P. L., & Da Costa, G. S. 1981, *ApJ*, 245, 79
- Cowley, A. P. & Hartwick, F. D. A. 1982, *ApJ*, 259, 89
- Cunha, K., Smith, V. V., Suntzeff, N. B., Norris, J. E., Da Costa, G. S., & Plez, B. 2002, *AJ*, 124, 379
- Den Hartog, E. A., Lawler, J. E., Sneden, C., Cowan, J. J. 2003, *ApJS*, 148, 543
- Denissenkov, P. A. & Herwig, F. 2003, *ApJ*, 590, 99
- Denissenkov, P. A. & Vandenberg, D. A. 2003, *ApJ*, 593, 509
- Denissenkov, P. A. & Weiss, A. 1996, *A&A*, 308, 773
- Dinescu, D. I., Girard, T. M., & van Altena, W. F. 1999, *AJ*, 117, 1792
- Dinescu, D. I., Majewski, S. R., Girard, T. M., & Cudworth, K. M. 2000, *AJ*, 120, 1892
- Domínguez, I., Höflich, P. & Straniero, O. 2001, *ApJ*, 557, 279
- Fitzpatrick, M. J. & Sneden, C. 1987, *BAAS*, 19, 1129
- Fuhr, J. R., Martin, G. A., & Wiese, W. L. 1988, *J. Phys. Chem. Ref. Data*, 17, 4
- Fulbright, J. P. 2000, *AJ*, 120, 1841
- Fulbright, J. P. 2002, *AJ*, 123, 404
- Fulbright, J. P. 2004, in *Carnegie Observatories Astrophysics Series, Vol. 4: Origin and Evolution of the Elements*, ed. A. McWilliam and M. Rauch (Pasadena: Carnegie Observatories, <http://www.ociw.edu/ociw/symposia/series/symposium4/proceedings.html>)
- Fulbright, J. P. & Johnson, J. A. 2003, *ApJ*, 595, 1154
- Fusi Pecci, F., Bellazzini, M., Cacciari, C., & Ferraro, F. R. 1995, *AJ*, 110, 1664
- Garz, T. 1973, *A&A*, 26, 471
- Geisler, D., Smith, V. V., Wallerstein, G., Gonzalez, G., & Charbonnel, C. 2005, *AJ*, 129, 1428
- Gonzalez, G. & Wallerstein, G. 1998, *AJ*, 116, 765
- Gratton, R. G. 1989, *A&A*, 208, 171
- Gratton, R. G., et al. 2001, *A&A*, 369, 87
- Gratton, R. G., Carretta, E., Eriksson, K., & Gustafsson, B. 1999, *A&A*, 350, 955
- Gratton, R. G. & Sneden, C. 1991, *A&A*, 241, 501
- Gratton, R. G., Sneden, C., & Carretta, E. 2004, *ARA&A*, 42, 385
- Grevesse, N., Blackwell, D. E., & Petford, A. D. 1989, *A&A*, 208, 157
- Grevesse, N., & Sauval, A. J. 1998, *Sp. Sci. Rev.*, 85, 161
- Gustafsson, B., Edvardsson, B., Eriksson, K., Mizuno-Wiedner, M., Jørgensen, U. G., & Plez, B. 2002, *ASP Conf. Ser. Vol 288*, ed. I. Hubeny, D. Mihalas, & K. Werner (San Francisco: ASP) 331.
- Hannaford, P., Lowe, R. M., Grevesse, N., Biémont, E., & Whaling, W. 1982, *ApJ*, 261, 736
- Hanson, R. B., Sneden, C., Kraft, R. P., & Fulbright, J. 1998, *AJ*, 116, 1286
- Heise, C. & Kock, M. 1990, *A&A*, 230, 244
- Hesser, J. E. 1978, *ApJ*, 223, L117
- Hesser, J. E. & Bell, R. A. 1980, *ApJ*, 238, L149
- Hill, V., Francois, P., Spite, M., Primas, F., & Spite, F. 2000, *A&A*, 364, 19
- Hill, V., Pompeia, L., & Spite, M. in press, in, "Chemical abundances and mixing in stars in the Milky Way and its satellites", ed. L. Pasquini & S. Randich, Springer Verlag Astrophysics Series
- Höflich, P. A., Gerardy, C. L., Fesen, R. A. & Sakai, S. 2002, *ApJ*, 568, 791
- Höflich, P. A., & Khokhlov, A. 1996, *ApJ*, 457, 500
- Höflich, P. A., Khokhlov, A. M. & Wheeler, J. C. 1995, *ApJ*, 444, 831
- Höflich, P. A., Wheeler, J. C. & Thielemann, F. K. 1998, *ApJ*, 495, 629
- Houdashelt, M. L., Bell, R. A., & Sweigart, A. V. 2000, *AJ*, 119, 1448
- Ibata, R. A., Gilmore, G., & Irwin, M. J. 1994, *Nature*, 370, 194
- Ibata, R. A., Gilmore, G., & Irwin, M. J. 1995, *MNRAS*, 277, 781
- Ivans, I. I. in press, in, "Chemical abundances and mixing in stars in the Milky Way and its satellites", ed. L. Pasquini & S. Randich, Springer Verlag Astrophysics Series
- Ivans, I. I., Kraft, R. P., Sneden, C., Smith, G. H., Rich, R. M., & Shetrone, M. 2001, *AJ*, 122, 1438 [M5-I01]
- Ivans, I. I., Sneden, C., James, C. R., Preston, G. W., Fulbright, J. P., Höflich, P. A., Carney, B. W., & Wheeler, J. C. 2003, *ApJ*, 592, 905
- Ivans, I. I., Sneden, C., Kraft, R. P., Suntzeff, N. B., Smith, V. V., Langer, G. E., & Fulbright, J. P. 1999, *AJ*, 118, 1273 [M4-I99]
- Iwamoto, K., Brachwitz, F., Nomoto, K., Kishimoto, N., Umeda, H., Hix, W. R. & Thielemann, F.-K. 1999, *ApJS*, 125, 439
- James, G. et al. 2004, *A&A*, 414, 107
- Johnson, C. I., Kraft, R. P., Pilachowski, C. A., Sneden, C., Ivans, I. I., & Benman G. 2005, *PASP*, in press
- Johnson, J. A. 2002, *ApJS*, 139, 219
- Johnson, J. A., Bolte, M., Stetson, P. B., Hesser, J. E., Somerville, R. S. 1999, *ApJ*, 527, 199 [LMC-J99]
- Kastberg, A., Villemoes, P., Arnesen, A., Heijkenskjöld, F., & Langereis, A. 1993, *J. Opt. Soc. Am. B*, 10, 1330
- Korn, A. 2004 in *Carnegie Observatories Astrophysics Series, Vol. 4: Origin and Evolution of the Elements*, ed. A. McWilliam and M. Rauch (Pasadena: Carnegie Observatories, <http://www.ociw.edu/ociw/symposia/series/symposium4/proceedings.html>)
- Kraft, R. P., & Ivans, I. I. 2003, *PASP*, 115, 143 [Fe-KI03]
- Kraft, R. P., & Ivans, I. I. 2004, in *Carnegie Observatories Astrophysics Series, Vol. 4: Origin and Evolution of the Elements*, ed. A. McWilliam and M. Rauch (Pasadena: Carnegie Observatories, <http://www.ociw.edu/ociw/symposia/series/symposium4/proceedings.html>) [Fe-KI04]
- Kraft, R. P., Sneden, C., Langer, G. E., & Shetrone, M. D. 1993, *AJ*, 106, 1490
- Kraft, R. P., Sneden, C., Langer, G. E., & Prosser, C. F. 1992, *AJ*, 104, 645
- Kraft, R. P., Sneden, C., Langer, G. E., Shetrone, M. D., & Bolte, M. 1995, *AJ*, 109, 2586
- Kraft, R. P., Sneden, C., Smith, G. H., Shetrone, M. D., & Fulbright, J. 1998, *AJ*, 115, 1500
- Kroll, S., & Kock, M. 1987, *A&AS*, 67, 225
- Kurucz, R. L. 1992, *Rev. Mex. Astron. Astrofis.*, 23, 181
- Kurucz, R. L. 1993, *ATLAS9 Stellar Atmosphere Programs and 2 km/s Grid*, Kurucz CD-ROM #13, Cambridge, MA: Smithsonian Astrophysical Observatory
- Kurucz, R. L., & Bell, B. 1995, *1995 Atomic Line Data*, Kurucz CD-ROM #23, Cambridge, MA: Smithsonian Astrophysical Observatory
- Langer, G. E., Hoffman, R. E., & Zaidins, C. S. 1997, *PASP*, 109, 244
- Lawler, J. E. & Dakin, J. T. 1989, *J. Opt. Soc. Am. B*, 6, 1457
- Lawler, J. E., Bonvallet, G., & Sneden, C. 2001, *ApJ*, 556, 452
- Lawler, J. E., Wickliffe, M. W., den Hartog, E. A., & Sneden, C. 2001, *ApJ*, 563, 1075
- Lefébvre, P.-H., Garnir, H.-P., & Biémont, E. 2003, *A&A*, 404, 1153
- Lee, J.-W. & Carney, B. W. 2002, *AJ*, 124, 1151
- Lee, J.-W., Carney, B. W., & Habgood, M. J. 2004, *AJ*, in press (astro-ph/0409706)
- Lin, D. N. C. & Richer, H. B. 1992, *ApJ*, 388, L57
- Lindblad, B. 1922, *ApJ*, 55, 85
- Lloyd Evans, T. 1980, *MNRAS*, 193, 87
- Mansour, N. B., Dinneen, T., Young, L., & Cheng, K. T. 1989, *Phys. Rev. A*, 39, 5762
- Martin, G. A., Fuhr, J. R., & Wiese, W. L. 1988, *J. Phys. Chem. Ref. Data*, 17, 3
- Mashonkina, L. I., Shimanskiĭ, V. V., & Sakhিবullin, N. A. 2000, *Astronomy Reports*, 44, 790, trans. from 2000, *Astron. Zh.*, 77 893
- Matteucci, F., Raiteri, C. M., Busso, M., Gallino, R., & Gratton, R. 1993, *A&A*, 272, 421
- Matteucci, F. & Recchi, S. 2001, *ApJ*, 558, 351
- May, M., Richter, J., & Wichelmann, J. 1974, *A&AS*, 18, 405
- McWilliam, A. 1997, *ARA&A*, 35, 503
- McWilliam, A., Preston, G. W., Sneden, C., & Searle, L. 1995, *AJ*, 109, 2757
- McWilliam, A., Rich, R. M., & Smecker-Hane, T. A. 2003, *ApJ*, 592, L21
- McWilliam, A. & Smecker-Hane, T. A. 2005, *ApJ*, 622, L29
- Messenger, B. B., & Lattanzio, J. C. 2002, *MNRAS*, 331, 684
- Mighell, K. J., Rich, R. M., Shara, M., & Fall, S. M. 1996, *AJ*, 111, 2314

- Mishenina, T. V., Kovtyukh, V. V., Soubiran, C., Travaglio, C., & Busso, M. 2002, *A&A*, 396, 189
- Nakamura, T., Umeda, H., Iwamoto, K., Nomoto, K., Hashimoto, M., Hix, W. R., Thielemann, F.-K. 2001, *ApJ*, 555, 880
- Nissen, P. E. & Schuster W. J. 1997, *A&A*, 326, 751 [NS97]
- Nitz, D. E., Kunau, A. E., Wilson, K. L., & Lentz, L. R. 1999, *APJS*, 122, 557
- Nitz, D. E., Wickliffe, M. E. & Lawler, J. E. 1998, *ApJS*, 117, 313
- O'Brian, T. R., Wickliffe, M. E., Lawler, J. E., Whaling, W., & Brault, J. W. 1991, *J. Opt. Soc. Am. B*, 8, 1185
- Olsen, K. A. G., Hodge, P. W., Mateo, M., Olszewski, E. W., Schommer, R. A., Suntzeff, N. B., & Walker, A. R. 1998, *MNRAS*, 300, 665 [LMC-O98]
- Olszewski, E. W., Schommer, R. A., Suntzeff, N.B., & Harris, H. C. 1991, *AJ*, 101, 515 [LMC-O91]
- Osborn, W. 1971, *Observatory*, 91, 223
- Palmeri, P., Biémont, E., Abousaïd, & Godefroid, M. 1995, *J. Phys. B*, 28, 3741
- Peterson, R. C. 1980, *ApJ*, 237, L87
- Pickering, J. C. 1996, *ApJS*, 107, 811
- Pickering, J. C., Thorne, A. P., & Perez, R. 2001, *ApJS*, 132, 403
- Pilachowski, C. A., Sneden, C., & Wallerstein, G. 1983, *ApJS*, 52, 241
- Popper, D. M. 1947, *ApJ*, 105, 204
- Prochaska, J. X., Naumov, S. O., Carney, B. W., McWilliam, A., & Wolfe, A. M. 2000, *AJ*, 120, 2513
- Ramírez, S. V. & Cohen, J. G. 2002, *AJ*, 123, 3277
- Ryan, S. G., Norris, J. E. & Beers, T. C. 1996, *ApJ*, 471, 254
- Salpeter, E. E. 1955, *ApJ*, 121, 161
- Sarajedini, A. 1994, *AJ*, 107, 618
- Schnabel, R., Kock, M., & Holweger, H. 1999, *A&A*, 342, 610
- Searle, L., Wilkinson, A., & Bagnuolo, W. G. 1980, *ApJ*, 239, 803
- Searle, L., & Zinn, R. 1978, *ApJ*, 225, 357
- Shetrone, M. D., Côté, P., & Sargent, W. L. W. 2001, *ApJ*, 548, 592 [dSph-S01]
- Shetrone, M. D. & Keane, M. J. 2000, *AJ*, 119, 840
- Shetrone, M. D., Venn, K. A., Tolstoy, E., Primas, F., Hill, V., & Kaufer, A. 2003, *AJ*, 125, 684
- Simmerer, J., Sneden, C., Ivans, I. I., Kraft, R. P., Shetrone, M. D., & Smith, V. V. 2003, *AJ*, 125, 2018
- Smecker-Hane, T. & McWilliam, A. 2004, *ApJ*, submitted
- Smith, G. & Raggett, D. St. J. 1981, *J. Phys. B.*, 14, 4015
- Smith, G. H., Sneden, C., & Kraft, R. P. 2002, *AJ*, 123, 1502
- Smith, V. et al. 2002, *AJ*, 124, 3241
- Sneden, C. 1973, *ApJ*, 184, 839
- Sneden, C. & Crocker, D. A. 1988, *ApJ*, 335, 406
- Sneden, C., Kraft, R. P., Guhathakurta, P., Peterson, R. C., & Fulbright, J. P. 2004, *AJ*, 127, 2162
- Sneden, C., Kraft, R. P., Shetrone, M. D., Smith, G. H., Langer, G. E., & Prosser, C. F. 1997, *AJ*, 114, 1964
- Stephens, A. 1999, *AJ*, 117, 1771
- Stetson, P. B., Hesser, J. E., Smith, G. H., Vandenberg, D. A., & Bolte, M. 1989, *AJ*, 97, 1360
- Sweigart, A. V. & Mengel, J. G. 1979, *ApJ*, 229, 624
- Takeda, Y., Zhao, G., Takada-Hidai, M., Chen, Y.-Q., Saito, Y., & Zhang, H.-W. 2003, *Chin. J. Astron. Astrophys.*, 3, 316
- Tautvaišienė, G., Wallerstein, G., Geisler, D., Gonzalez, G., & Charbonnel, C. 2004, *AJ*, 127, 373
- Testa, V., Ferraro, F. R., Brocato, E., & Castellani, V. 1995, *MNRAS*, 275, 454
- Timmes, F. X., Woosley, S. E., & Weaver, T. A. 1995, *ApJS*, 998, 617
- Tinsley, B. M. 1979, *ApJ*, 229, 1046
- Tolstoy, E., Venn, K., Shetrone, M., Primas, F., Hill, V., Kaufer, A., & Szeifert, T. 2003, *AJ*, 125, 707
- Tozzi, G. P., Brunner, A. J., & Huber, M. C. E. 1985, *MNRAS*, 217, 423
- Truran, J. W. 1981, *A&A*, 97, 391
- van den Bergh, S. 1967, *AJ*, 72, 70
- Whaling, W., Hannaford, P., Lowe, R. M., Biémont, E., & Grevesse, N. 1985, *A&A*, 153, 109
- Wickliffe, M. E. & Lawler, J. E. 1997, *ApJS*, 110, 163
- Woosley, S. E. & Weaver, T. A. 1995, *ApJS*, 101, 181

Table 2. Equivalent Widths

Wavelength Å	Species	E.P. eV	log gf	N1898 #1	N1898 #2	N2005 #1	N2005 #2	N2005 #3	N2019 #1	N2019 #2	N2019 #3	Hodge11 #1	Hodge11 #2	Source	EW or SYN
6300.31	O I	0.00	-9.75	59.5	...	43.7	64.9	56.5	51.4	1	SYN
6363.79	O I	0.02	-10.25	24.3	27.5	1	SYN
5682.65	Na I	2.10	-0.70	56.8	102.9	56.0	49.1	57.6	90.7	1	SYN
5688.22	Na I	2.10	-0.46	75.5	133.2	66.5	...	49.4	66.8	90.5	105.3	1	SYN
5172.70	Mg I	2.71	-0.39	382.6	363.2	371.2	318.6	2	EW
5183.60	Mg I	2.70	-0.17	422.5	390.2	377.5	2	EW
5528.42	Mg I	4.34	-0.36	209.5	204.6	180.1	166.9	162.3	192.2	207.9	204.8	120.8	143.2	1	EW
5711.09	Mg I	4.34	-1.63	100.6	105.9	67.4	...	58.8	122.8	118.9	116.3	...	48.1	1	EW
6696.03	Al I	3.14	-1.57	...	99.5	29.9	1	EW
6698.67	Al I	3.14	-1.89	...	60.5	1	EW
5684.55	Si I	4.95	-1.65	35.5	43.8	3	SYN
5690.43	Si I	4.93	-1.87	33.3	67.7	...	27.0	3	EW
5793.08	Si I	4.93	-2.06	29.0	36.5	1	SYN
5948.55	Si I	5.08	-1.23	45.8	58.0	58.1	3	EW
5581.98	Ca I	2.52	-0.71	111.5	121.3	96.2	82.9	78.5	114.1	124.2	130.3	...	53.2	4	EW
5588.76	Ca I	2.53	0.21	162.8	179.0	151.7	117.1	...	163.5	169.6	191.1	104.1	109.1	4	EW
5601.29	Ca I	2.53	-0.52	114.8	138.9	81.7	68.9	86.7	114.7	115.3	124.7	53.7	63.3	5	EW
6102.73	Ca I	1.88	-0.79	170.4	216.8	144.1	...	98.8	170.6	172.2	...	82.8	105.3	6	EW
6122.23	Ca I	1.89	-0.32	206.4	249.3	188.8	139.8	170.2	214.0	196.1	243.2	131.3	147.2	6	EW
6162.15	Ca I	1.90	-0.09	214.9	258.8	197.3	148.4	181.4	210.1	209.2	264.5	135.4	149.3	6	EW
6166.44	Ca I	2.52	-1.14	81.9	94.0	56.3	76.1	73.6	93.3	5	EW
6439.08	Ca I	2.52	0.39	192.6	212.4	173.1	145.6	153.4	201.0	191.3	200.2	125.6	143.0	5	EW
6449.82	Ca I	2.52	-0.50	153.7	166.8	102.0	111.9	98.9	115.5	134.3	123.1	72.0	65.9	5	EW
6471.67	Ca I	2.53	-0.69	128.5	136.3	88.8	...	83.7	122.2	103.6	133.1	55.9	57.7	5	EW
6493.78	Ca I	2.52	-0.11	147.8	...	127.0	92.7	108.2	147.2	147.8	169.0	68.5	81.7	5	EW
6499.65	Ca I	2.52	-0.82	124.4	128.5	...	55.4	71.0	114.3	150.3	116.6	...	43.9	5	EW
6717.69	Ca I	2.71	-0.61	130.7	...	105.1	59.7	...	137.8	137.2	143.4	51.2	51.4	7	EW
7148.15	Ca I	2.71	0.25	164.1	202.4	152.3	129.3	127.7	171.8	163.1	201.1	108.8	116.3	7	EW
7202.21	Ca I	2.71	-0.01	146.2	151.2	118.3	109.0	110.3	148.7	135.5	152.5	60.1	82.2	7	EW
5526.82	Sc II	1.77	0.02	...	115.4	123.1	101.0	87.2	101.6	118.5	101.4	106.9	87.3	8	EW
5640.99	Sc II	1.50	-1.13	...	77.5	55.8	69.2	...	58.5	66.7	75.8	...	39.6	8	EW
5657.88	Sc II	1.51	-0.60	...	133.9	107.0	81.6	96.4	140.8	89.7	118.0	62.8	65.8	8	EW
5667.15	Sc II	1.50	-1.36	...	83.9	70.8	43.3	8	EW
6245.62	Sc II	1.51	-1.07	...	89.7	73.8	49.7	38.2	69.6	76.0	71.0	39.1	40.1	1	EW
6604.60	Sc II	1.36	-1.31	...	101.9	54.5	53.3	42.4	76.3	65.3	69.1	...	32.2	8	EW
4926.15	Ti I	0.82	-2.11	58.6	71.9	57.8	54.2	9	EW

Table 2—Continued

Wavelength Å	Species	E.P. eV	log gf	N1898 #1	N1898 #2	N2005 #1	N2005 #2	N2005 #3	N2019 #1	N2019 #2	N2019 #3	Hodge11 #1	Hodge11 #2	Source	EW or SYN
4928.36	Ti I	2.15	0.05	59.4	71.6	10	EW
5000.98	Ti I	2.00	-0.02	62.8	137.0	88.3	11	EW
5009.63	Ti I	0.02	-2.20	118.8	182.2	65.7	128.9	11	EW
5043.59	Ti I	0.84	-1.68	101.6	96.1	107.1	...	117.5	9	EW
5045.41	Ti I	0.84	-1.94	84.3	84.0	64.2	68.7	78.3	9	EW
5071.45	Ti I	1.46	-1.00	81.3	89.8	65.3	91.7	12	EW
5193.00	Ti I	0.02	-0.95	247.1	279.4	218.3	...	112.9	134.3	13	EW
5201.14	Ti I	2.09	-0.66	41.0	43.5	11	EW
5219.71	Ti I	0.02	-2.23	152.3	155.2	113.6	40.5	170.1	193.0	...	77.4	13	EW
5223.63	Ti I	2.09	-0.49	41.2	11	EW
5282.41	Ti I	1.05	-1.30	70.1	63.7	27.7	75.3	10	EW
5295.78	Ti I	1.07	-1.58	73.5	89.5	68.1	70.2	85.9	9	EW
5426.30	Ti I	0.02	-2.95	80.9	143.7	53.6	69.9	133.0	139.2	13	EW
5471.25	Ti I	1.44	-1.40	43.8	58.5	45.7	10	EW
5490.16	Ti I	1.46	-0.88	72.6	96.5	32.8	90.0	103.5	12	EW
5490.80	Ti I	0.05	-3.35	118.5	10	EW
5899.30	Ti I	1.05	-1.10	125.8	156.6	83.6	36.6	41.6	115.9	128.4	163.0	14	EW
5903.29	Ti I	1.07	-2.09	54.4	54.8	57.2	47.2	68.3	9	EW
5918.55	Ti I	1.07	-1.46	81.1	93.2	59.1	45.3	28.7	62.8	77.3	111.3	10	EW
5937.84	Ti I	1.07	-1.89	51.8	77.3	80.6	54.3	90.6	10	EW
5941.76	Ti I	1.05	-1.51	96.2	111.6	60.2	...	33.5	82.1	98.4	128.3	10	EW
5965.82	Ti I	1.89	-0.35	85.7	95.4	56.7	38.1	112.2	12	EW
5978.58	Ti I	1.87	-0.44	77.5	92.8	48.6	70.3	...	102.1	12	EW
6064.62	Ti I	1.05	-1.89	56.6	47.5	63.3	79.3	9	EW
6126.22	Ti I	1.07	-1.37	96.6	128.7	68.8	...	43.2	88.7	98.0	154.1	9	EW
6258.06	Ti I	1.44	-0.29	124.3	164.4	86.0	43.5	66.9	120.1	142.6	39.0	12	EW
6303.77	Ti I	1.44	-1.51	46.9	55.5	23.1	50.3	69.0	12	EW
6312.24	Ti I	1.46	-1.50	48.0	70.6	55.0	49.8	72.5	12	EW
6554.24	Ti I	1.44	-1.16	68.8	87.0	36.0	71.3	79.8	99.9	12	EW
6556.08	Ti I	1.46	-1.01	90.3	111.8	43.4	101.9	86.9	131.0	12	EW
6743.13	Ti I	0.90	-1.63	107.5	126.4	57.7	102.5	91.1	132.2	10	EW
7138.93	Ti I	1.44	-1.59	41.2	78.3	44.0	42.0	86.8	10	EW
7209.50	Ti I	1.46	-0.50	139.2	157.6	93.5	69.1	79.1	134.7	136.4	167.0	30.6	35.5	10	EW
7216.19	Ti I	1.44	-1.15	75.6	121.7	42.7	84.9	82.6	115.0	10	EW
4865.61	Ti II	1.12	-2.79	82.9	41.3	...	101.6	142.8	...	67.8	15	EW
5005.19	Ti II	1.57	-2.72	58.5	75.3	51.4	15	EW

Table 2—Continued

Wavelength Å	Species	E.P. eV	log gf	N1898 #1	N1898 #2	N2005 #1	N2005 #2	N2005 #3	N2019 #1	N2019 #2	N2019 #3	Hodge11 #1	Hodge11 #2	Source	EW or SYN
5185.90	Ti II	1.89	-1.49	104.7	99.2	93.9	109.5	89.9	131.4	131.9	150.3	...	98.7	15	EW
5381.03	Ti II	1.57	-1.92	127.3	152.9	123.1	120.9	89.4	...	138.1	173.2	101.2	102.8	15	EW
5418.77	Ti II	1.58	-2.11	107.8	109.7	91.0	83.9	77.1	73.0	...	83.0	...	74.3	2	EW
6559.58	Ti II	2.05	-2.13	57.2	77.6	50.8	...	62.8	63.5	44.6	69.2	...	33.1	4	EW
7214.74	Ti II	2.59	-1.74	32.9	41.3	25.8	34.1	43.3	56.5	10	EW
4851.47	V I	0.00	-1.14	...	186.3	166.8	196.3	16	EW
6039.73	V I	1.06	-0.65	...	77.8	69.3	80.4	16	EW
6081.43	V I	1.05	-0.58	33.1	61.1	55.2	81.0	16	EW
6090.21	V I	1.08	-0.06	87.7	103.9	141.0	16	EW
6111.59	V I	1.04	-0.72	...	92.0	19.3	62.4	46.0	102.0	16	EW
6119.50	V I	1.06	-0.32	...	112.4	50.6	...	88.6	91.5	72.7	108.9	16	EW
6135.35	V I	1.05	-0.75	...	83.8	46.1	66.0	89.6	16	EW
6150.17	V I	0.03	-1.78	...	123.7	50.4	78.5	82.0	138.4	10	EW
6199.14	V I	0.29	-1.30	...	164.6	62.6	112.9	102.4	174.2	16	EW
6216.43	V I	0.28	-1.29	...	159.3	61.7	...	39.3	129.3	113.9	157.2	16	EW
6224.47	V I	0.29	-2.01	...	106.9	25.2	65.6	74.2	99.7	10	EW
6233.17	V I	0.28	-2.07	...	77.2	39.4	68.7	97.9	10	EW
6251.76	V I	0.29	-1.34	...	133.9	49.7	94.4	107.2	116.0	16	EW
6274.64	V I	0.27	-1.67	...	101.4	28.7	73.4	...	104.1	16	EW
6285.11	V I	0.28	-1.51	...	126.6	64.2	94.1	75.8	121.1	16	EW
5204.47	Cr I	0.94	-0.21	357.6	222.9	...	322.0	...	173.6	215.5	17,18	EW
5296.70	Cr I	0.98	-1.40	170.9	220.2	157.2	...	100.0	156.5	177.9	226.2	...	94.1	17,18	EW
5345.79	Cr I	1.00	-0.98	191.6	238.3	173.8	...	153.4	210.2	204.7	221.8	111.1	114.1	17,18	EW
5348.34	Cr I	1.00	-1.29	178.2	210.9	161.0	198.2	178.5	198.1	109.8	96.5	17,18	EW
5783.07	Cr I	3.32	-0.30	47.7	30.8	29.8	40.5	53.2	10	EW
5783.87	Cr I	3.32	-0.08	70.4	74.5	58.7	68.7	58.1	10	EW
5787.93	Cr I	3.32	-0.08	61.6	66.6	46.5	35.8	86.4	18	EW
6330.10	Cr I	0.94	-2.92	104.0	130.7	58.1	...	36.2	102.5	86.4	108.8	10	EW
5394.67	Mn I	0.00	-3.50	19	SYN
5420.27	Mn I	2.14	-1.46	19	SYN
5432.53	Mn I	0.00	-3.80	...	205.0	142.8	...	76.1	161.7	191.0	206.1	19	EW
5516.69	Mn I	2.18	-1.85	19	SYN
6013.52	Mn I	3.07	-0.25	...	125.5	24.9	80.7	87.9	101.1	19	EW
6021.71	Mn I	3.07	0.03	...	113.8	64.2	46.4	33.8	115.7	109.8	108.4	19	EW
4859.70	Fe I	2.88	-0.76	171.8	193.1	109.3	...	204.6	166.8	...	119.7	20	EW
4871.36	Fe I	2.87	-0.36	174.4	317.0	...	131.3	159.2	208.9	...	107.9	20	EW

Table 2—Continued

Wavelength Å	Species	E.P. eV	log gf	N1898 #1	N1898 #2	N2005 #1	N2005 #2	N2005 #3	N2019 #1	N2019 #2	N2019 #3	Hodge11 #1	Hodge11 #2	Source	EW or SYN
4891.52	Fe I	2.84	-0.11	233.2	316.9	163.0	213.8	...	217.6	...	154.9	20	EW
4917.23	Fe I	4.19	-1.18	74.2	21	EW
4924.77	Fe I	2.28	-2.25	169.4	216.5	...	119.6	109.7	...	148.7	149.2	...	89.9	22	EW
4950.11	Fe I	3.42	-1.67	104.4	55.9	...	95.9	23	EW
4969.93	Fe I	4.22	-0.71	98.8	107.7	74.4	23	EW
4994.14	Fe I	0.92	-3.04	219.1	246.4	...	126.1	139.5	223.0	203.9	273.3	167.6	163.4	24	EW
5001.82	Fe I	3.88	0.01	119.9	110.7	149.5	139.5	145.1	...	76.9	23	EW
5014.93	Fe I	3.94	-0.30	127.7	107.2	142.6	...	107.2	20	EW
5068.77	Fe I	2.94	-1.04	142.9	203.8	...	124.4	93.9	156.3	129.3	161.4	...	115.7	20	EW
5083.33	Fe I	0.96	-2.92	241.8	286.3	...	130.0	149.6	216.8	198.7	194.7	148.5	166.7	24	EW
5090.77	Fe I	4.26	-0.40	...	87.2	90.7	...	80.5	...	48.4	23	EW
5133.66	Fe I	4.18	0.14	120.5	106.4	61.7	165.1	141.3	142.4	...	96.3	23	EW
5141.72	Fe I	2.42	-1.96	155.2	190.5	117.4	89.0	119.1	153.7	152.3	146.9	...	87.5	22	EW
5143.73	Fe I	2.20	-3.79	91.4	...	59.5	61.0	21	EW
5162.30	Fe I	4.18	0.02	134.7	114.4	117.1	...	98.7	150.6	107.2	124.3	91.3	83.1	23	EW
5169.00	Fe I	0.05	-3.97	446.8	...	331.5	25	EW
5198.72	Fe I	2.22	-2.13	179.7	183.3	173.0	...	122.2	168.6	169.0	171.3	112.4	95.9	26	EW
5202.33	Fe I	2.19	-1.84	208.7	247.4	198.3	127.7	163.7	224.1	166.5	209.7	111.8	132.5	20	EW
5215.19	Fe I	3.27	-0.87	164.4	163.4	154.1	77.4	93.0	132.8	...	177.2	...	82.0	27	EW
5217.42	Fe I	3.21	-1.07	138.6	150.9	116.8	...	96.0	146.0	162.2	143.5	...	76.4	22	EW
5223.15	Fe I	3.64	-1.78	32.9	20	EW
5225.50	Fe I	0.11	-4.76	240.4	256.0	216.5	127.0	161.2	226.2	211.9	235.0	124.9	...	20	EW
5232.97	Fe I	2.94	-0.10	253.4	262.6	212.6	...	177.1	251.4	206.8	200.4	144.5	160.4	27	EW
5242.46	Fe I	3.62	-0.97	124.3	...	96.9	...	63.2	126.1	108.6	103.2	...	47.1	20	EW
5243.78	Fe I	4.26	-1.05	74.3	60.1	36.9	...	44.3	70.7	52.0	44.9	21	EW
5253.42	Fe I	3.28	-1.57	112.5	117.0	76.2	63.1	...	103.0	91.3	90.1	...	46.6	27	EW
5263.28	Fe I	3.27	-0.88	166.1	184.4	137.9	...	115.8	184.6	144.4	173.9	106.6	86.8	22	EW
5281.74	Fe I	3.04	-0.83	174.0	...	161.3	138.8	121.5	191.2	162.7	162.0	86.5	93.7	20	EW
5288.52	Fe I	3.68	-1.51	86.4	97.9	58.8	77.6	83.3	20	EW
5307.36	Fe I	1.61	-2.99	171.1	175.4	159.6	101.8	161.0	164.7	175.2	170.6	109.9	100.4	28	EW
5322.01	Fe I	2.28	-2.80	139.6	116.0	107.4	...	75.3	99.2	126.5	114.8	...	38.0	20	EW
5324.15	Fe I	3.21	-0.22	210.1	233.2	194.2	150.8	156.3	184.2	216.1	223.6	130.9	127.8	21	EW
5332.92	Fe I	1.56	-2.78	219.2	253.2	195.0	129.7	147.1	196.1	206.1	217.8	126.2	130.0	20	EW
5364.87	Fe I	4.45	0.23	124.3	113.4	100.4	67.9	104.9	111.1	106.4	121.7	...	66.0	20	EW
5365.40	Fe I	3.56	-1.02	109.8	134.4	88.9	48.8	83.5	107.5	99.5	105.1	...	51.0	20	EW
5367.49	Fe I	4.42	0.44	119.1	144.6	107.9	82.6	114.3	126.0	117.6	140.1	50.1	60.8	27	EW

Table 2—Continued

Wavelength Å	Species	E.P. eV	log gf	N1898 #1	N1898 #2	N2005 #1	N2005 #2	N2005 #3	N2019 #1	N2019 #2	N2019 #3	Hodge11 #1	Hodge11 #2	Source	EW or SYN
5373.69	Fe I	4.47	-0.76	62.0	69.3	37.8	73.6	87.3	57.8	21	EW
5379.51	Fe I	3.69	-1.51	83.3	92.4	61.0	...	51.7	66.6	59.5	89.7	20	EW
5383.38	Fe I	4.31	0.64	142.4	170.4	157.8	97.7	97.8	140.2	137.3	146.3	61.1	85.1	20	EW
5389.48	Fe I	4.42	-0.41	...	139.8	...	53.7	63.0	107.8	86.6	115.5	...	40.2	23	EW
5410.92	Fe I	4.45	0.40	123.6	131.6	96.4	84.6	75.4	99.3	103.6	107.4	71.4	52.6	20	EW
5415.21	Fe I	4.37	0.64	140.0	149.1	123.9	98.1	99.9	183.8	157.6	129.0	105.8	90.1	20	EW
5424.08	Fe I	4.32	0.52	135.3	197.7	144.9	131.0	123.4	...	160.9	126.8	117.7	111.4	23	EW
5434.53	Fe I	1.01	-2.08	307.4	316.4	262.7	182.8	214.2	290.8	274.8	310.0	181.9	209.4	24	EW
5445.05	Fe I	4.39	-0.02	114.9	126.7	101.3	49.6	88.6	116.8	89.0	109.8	66.1	83.9	23	EW
5501.48	Fe I	0.96	-3.05	262.1	275.1	235.7	165.0	168.6	195.8	262.6	287.7	166.2	164.7	1	EW
5522.45	Fe I	4.21	-1.45	...	43.9	28.8	...	26.0	21	EW
5525.55	Fe I	4.23	-1.23	65.0	72.4	46.3	21	EW
5543.94	Fe I	4.22	-1.04	65.1	77.0	52.1	60.2	21	EW
5560.21	Fe I	4.43	-1.09	40.4	53.2	25.5	21	EW
5567.40	Fe I	2.61	-2.56	118.4	139.2	90.0	58.2	79.9	99.3	98.9	128.9	22	EW
5569.62	Fe I	3.42	-0.49	160.1	177.0	156.9	91.3	127.0	160.2	153.2	183.2	88.9	110.6	27	EW
5576.09	Fe I	3.43	-0.90	145.6	162.2	...	84.9	103.3	130.2	113.3	138.8	83.6	82.1	21	EW
5586.77	Fe I	3.37	-0.20	190.6	217.1	171.7	137.6	139.6	183.7	196.8	196.6	121.2	119.3	21	EW
5618.64	Fe I	4.21	-1.28	55.7	65.2	37.3	20	EW
5619.61	Fe I	4.39	-1.60	31.7	44.8	21.6	21	EW
5633.95	Fe I	4.99	-0.23	54.9	55.7	41.7	21	EW
5638.27	Fe I	4.22	-0.77	90.0	91.2	56.3	80.4	21	EW
5641.45	Fe I	4.26	-1.08	85.2	70.8	49.1	55.4	65.7	21	EW
5717.84	Fe I	4.28	-1.03	67.8	81.4	...	39.1	...	77.8	...	73.8	21	EW
5731.77	Fe I	4.26	-1.20	57.8	76.7	43.6	60.1	48.6	62.8	21	EW
5775.06	Fe I	4.22	-1.30	60.9	67.1	39.2	69.1	66.4	65.1	20	EW
5816.38	Fe I	4.55	-0.60	69.7	93.6	43.1	...	71.1	73.7	76.1	20	EW
5852.23	Fe I	4.55	-1.23	50.8	62.1	38.3	...	36.7	21	EW
5934.72	Fe I	3.93	-1.07	115.5	115.7	67.8	...	50.6	121.1	...	141.6	...	28.1	21	EW
5956.70	Fe I	0.86	-4.61	158.7	188.1	143.2	118.7	83.1	158.3	...	196.0	81.2	77.0	24	EW
6003.02	Fe I	3.88	-1.12	99.5	109.7	73.7	51.6	49.3	95.7	87.3	123.5	...	39.2	23	EW
6020.19	Fe I	4.61	-0.27	116.2	110.9	70.4	...	42.7	98.2	98.1	98.3	...	40.3	23	EW
6024.07	Fe I	4.55	-0.12	103.8	109.7	75.6	51.7	48.8	105.5	96.8	103.5	43.7	43.3	23	EW
6027.07	Fe I	4.08	-1.21	73.4	85.3	53.2	37.9	31.4	55.8	58.9	76.8	21	EW
6056.01	Fe I	4.73	-0.46	55.2	...	38.7	63.7	38.7	63.0	23	EW
6065.49	Fe I	2.61	-1.49	188.5	...	163.9	148.9	107.2	160.5	177.5	200.2	108.5	125.6	29	EW

Table 2—Continued

Wavelength Å	Species	E.P. eV	log gf	N1898 #1	N1898 #2	N2005 #1	N2005 #2	N2005 #3	N2019 #1	N2019 #2	N2019 #3	Hodge11 #1	Hodge11 #2	Source	EW or SYN
6120.25	Fe I	0.91	-5.97	63.5	75.0	45.8	42.6	62.8	81.4	23	EW
6136.63	Fe I	2.44	-1.40	208.9	147.8	156.7	194.9	196.2	269.4	181.6	...	26	EW
6137.70	Fe I	2.59	-1.40	208.4	238.0	180.7	168.7	152.2	209.1	193.1	232.7	136.7	131.7	29	EW
6151.62	Fe I	2.18	-3.30	121.1	129.2	93.1	48.2	67.8	86.8	110.7	134.4	26	EW
6157.73	Fe I	4.08	-1.16	89.6	104.8	54.0	...	83.7	77.2	88.5	102.8	21	EW
6173.29	Fe I	2.22	-2.88	145.8	167.4	126.1	68.3	86.8	150.6	126.2	145.4	65.7	70.8	26	EW
6180.18	Fe I	2.73	-2.59	104.8	99.8	89.2	...	57.6	134.5	97.2	114.8	22	EW
6187.99	Fe I	3.94	-1.58	69.4	70.4	48.4	73.3	62.4	39.5	2	EW
6200.27	Fe I	2.61	-2.44	136.4	134.1	120.1	69.2	92.6	125.5	125.8	145.7	...	53.5	29	EW
6219.28	Fe I	2.20	-2.43	159.8	187.9	158.0	126.4	137.0	166.7	171.4	185.2	86.9	97.7	26	EW
6229.23	Fe I	2.84	-2.97	89.9	81.7	61.4	62.3	65.9	76.7	21	EW
6232.66	Fe I	3.65	-1.22	119.1	124.2	88.8	62.2	...	109.8	102.6	103.5	...	32.9	27	EW
6246.32	Fe I	3.60	-0.96	129.8	158.6	112.0	67.0	106.0	121.0	112.1	131.9	49.4	73.3	1	EW
6252.57	Fe I	2.40	-1.69	186.5	208.0	154.0	120.3	...	182.3	189.2	215.4	111.3	103.4	26	EW
6265.19	Fe I	2.18	-2.51	162.9	186.4	153.4	99.0	134.5	160.9	167.0	187.3	78.3	100.7	26	EW
6270.23	Fe I	2.86	-2.61	103.1	104.3	74.3	44.2	...	102.0	107.7	100.9	20	EW
6297.80	Fe I	2.22	-2.74	162.9	159.7	116.9	81.3	106.9	151.1	147.0	162.8	65.8	70.1	26	EW
6301.51	Fe I	3.65	-0.72	146.1	150.6	97.9	96.9	...	127.6	150.9	138.0	...	54.5	22	EW
6302.49	Fe I	3.69	-1.15	94.9	...	87.7	69.0	74.9	98.9	118.2	116.4	...	59.6	1	EW
6311.51	Fe I	2.83	-3.23	59.1	62.5	33.2	69.3	40.2	64.3	21	EW
6322.70	Fe I	2.59	-2.43	143.9	138.2	108.5	93.2	101.0	133.8	109.2	139.3	...	77.3	29	EW
6335.34	Fe I	2.20	-2.18	177.6	220.4	155.5	125.7	126.2	153.5	175.4	199.7	125.3	127.9	20	EW
6336.83	Fe I	3.69	-0.86	134.1	152.7	105.7	99.2	89.1	117.7	116.5	120.2	65.4	64.3	27	EW
6344.16	Fe I	2.43	-2.92	129.9	133.3	106.9	68.5	67.5	127.8	122.1	147.0	34.4	...	26	EW
6355.02	Fe I	2.84	-2.36	123.5	152.6	96.2	66.4	76.4	113.5	110.3	128.5	...	50.8	22	EW
6380.77	Fe I	4.19	-1.38	60.0	57.3	40.4	...	73.3	20	EW
6392.54	Fe I	2.28	-4.03	57.9	76.2	60.1	...	59.8	23	EW
6393.61	Fe I	2.43	-1.43	204.1	222.3	...	140.6	167.0	184.6	186.5	218.4	107.3	140.1	22	EW
6408.03	Fe I	3.69	-1.02	119.7	123.2	97.8	75.6	81.4	120.8	119.2	121.2	...	46.8	22	EW
6411.66	Fe I	3.65	-0.60	150.1	154.1	124.0	113.9	117.4	145.1	130.1	153.9	...	79.5	22	EW
6421.36	Fe I	2.28	-2.03	191.6	219.6	160.0	145.3	151.1	188.1	196.2	214.1	124.4	126.8	26	EW
6430.86	Fe I	2.18	-2.00	203.9	234.8	180.4	171.0	151.8	202.6	186.6	220.1	118.9	132.8	26	EW
6469.19	Fe I	4.83	-0.73	67.6	67.0	28.5	34.2	...	50.9	54.8	63.8	21	EW
6481.88	Fe I	2.28	-2.94	143.6	139.9	104.0	82.4	101.2	130.4	125.7	144.4	52.9	49.9	26	EW
6494.99	Fe I	2.40	-1.27	227.2	249.7	199.0	178.9	184.8	225.8	216.2	240.6	150.7	160.3	26	EW
6498.95	Fe I	0.96	-4.69	160.6	171.3	119.2	...	104.7	165.0	144.2	171.3	62.9	65.0	24	EW

Table 2—Continued

Wavelength Å	Species	E.P. eV	log gf	N1898 #1	N1898 #2	N2005 #1	N2005 #2	N2005 #3	N2019 #1	N2019 #2	N2019 #3	Hodge11 #1	Hodge11 #2	Source	EW or SYN
6518.33	Fe I	2.83	-2.30	101.4	127.6	73.5	...	76.1	99.8	99.2	111.7	20	EW
6569.22	Fe I	4.74	-0.38	79.4	83.0	72.9	...	58.5	83.9	92.3	77.2	21	EW
6574.25	Fe I	0.99	-5.00	142.7	157.4	104.3	57.2	89.5	123.7	141.7	152.7	...	48.3	21	EW
6575.04	Fe I	2.59	-2.71	131.0	145.2	99.4	72.6	...	123.4	123.5	138.0	41.7	41.5	20	EW
6581.22	Fe I	1.48	-4.86	109.1	124.9	73.5	42.8	...	82.1	91.4	113.6	...	28.9	21	EW
6593.88	Fe I	2.43	-2.42	149.5	173.6	137.4	97.0	134.6	140.8	137.4	174.8	66.5	88.2	26	EW
6608.04	Fe I	2.28	-4.04	61.0	88.2	37.6	55.7	65.4	70.1	21	EW
6609.12	Fe I	2.56	-2.66	127.2	163.6	107.4	83.6	86.7	115.9	99.6	127.1	...	48.9	20	EW
6678.00	Fe I	2.69	-1.47	207.2	216.2	182.6	140.9	166.6	184.0	167.3	192.4	96.4	121.2	23	EW
6703.58	Fe I	2.76	-3.06	76.2	87.1	73.3	94.7	58.2	86.2	21	EW
6710.32	Fe I	1.48	-4.88	93.9	92.3	70.2	80.5	94.9	89.0	23	EW
6726.73	Fe I	4.61	-1.07	39.4	52.3	29.5	7	EW
6739.52	Fe I	1.56	-4.95	74.3	95.8	45.1	60.5	55.8	72.3	23	EW
6750.16	Fe I	2.42	-2.58	143.7	172.6	130.5	88.9	103.9	128.7	126.1	157.9	68.6	72.0	20	EW
6806.88	Fe I	2.73	-3.21	75.6	98.8	54.5	84.1	68.7	101.3	23	EW
6810.27	Fe I	4.61	-0.99	52.4	40.5	30.7	51.9	81.5	44.7	20	EW
6828.59	Fe I	4.64	-0.82	67.9	45.8	21	EW
6839.84	Fe I	2.56	-3.35	75.1	96.5	51.9	73.1	58.2	21	EW
6842.69	Fe I	4.64	-1.22	35.6	45.8	30.0	21	EW
6843.65	Fe I	4.55	-0.83	52.4	64.2	60.2	50.0	21	EW
6857.25	Fe I	4.08	-2.05	29.6	31.4	21	EW
6858.16	Fe I	4.61	-0.93	50.5	60.4	20	EW
6916.69	Fe I	4.15	-1.35	84.0	83.8	28.6	21	EW
6945.20	Fe I	2.42	-2.45	147.6	162.1	135.2	91.7	108.6	130.0	140.9	170.4	71.2	82.4	20	EW
6971.97	Fe I	3.02	-3.49	44.3	40.7	23	EW
6988.53	Fe I	2.40	-3.56	73.8	89.4	64.9	...	40.5	70.6	71.7	79.8	21	EW
7014.99	Fe I	2.45	-4.20	41.2	23.1	32.8	23	EW
7022.96	Fe I	4.19	-1.15	65.1	88.2	39.4	...	53.9	61.3	49.4	68.6	21	EW
7038.22	Fe I	4.22	-1.20	60.5	85.9	51.8	58.3	59.1	58.6	21	EW
7090.39	Fe I	4.23	-1.11	81.4	73.1	40.4	...	58.9	52.4	53.7	78.7	21	EW
7112.17	Fe I	2.99	-2.99	59.6	88.5	39.3	40.8	58.9	21	EW
7130.93	Fe I	4.22	-0.75	89.4	112.8	72.2	...	62.4	78.2	92.6	103.9	...	33.5	21	EW
7132.99	Fe I	4.08	-1.63	44.0	41.4	37.4	35.8	38.9	57.4	20	EW
7151.46	Fe I	2.48	-3.66	52.5	84.4	42.9	26.8	32.8	54.7	66.2	74.1	23	EW
7180.00	Fe I	1.48	-4.75	98.3	...	54.4	41.0	52.4	87.3	109.5	109.9	23	EW
7181.17	Fe I	4.22	-1.25	65.2	...	44.2	43.3	54.0	75.6	7	EW

Table 2—Continued

Wavelength Å	Species	E.P. eV	log gf	N1898 #1	N1898 #2	N2005 #1	N2005 #2	N2005 #3	N2019 #1	N2019 #2	N2019 #3	Hodge11 #1	Hodge11 #2	Source	EW or SYN
7187.38	Fe I	4.10	-0.15	150.8	197.0	109.6	106.7	106.5	134.0	153.9	180.2	75.5	77.4	20	EW
7219.68	Fe I	4.08	-1.69	43.3	57.8	26.3	36.3	37.8	52.2	23	EW
7223.64	Fe I	3.02	-2.21	113.9	121.2	94.0	47.3	63.7	97.6	107.8	100.7	20	EW
7228.70	Fe I	2.76	-3.38	62.5	86.2	35.5	52.1	57.8	59.3	23	EW
4923.93	Fe II	2.89	-1.24	189.5	184.9	143.4	...	144.5	138.4	...	104.4	30	EW
5197.60	Fe II	3.23	-2.10	84.7	...	82.4	84.9	...	30	SYN
5234.64	Fe II	3.22	-2.22	96.8	101.9	...	115.7	...	55.5	75.1	31	EW
6149.25	Fe II	3.89	-2.72	34.8	30.6	29.6	1	EW
6416.93	Fe II	3.89	-2.85	40.1	33.4	30.5	38.8	23	EW
6432.68	Fe II	2.89	-3.51	43.0	33.6	34.6	36.7	41.6	32.3	...	42.3	37.0	27.6	31	EW
6456.39	Fe II	3.90	-2.30	43.7	30.8	46.7	50.5	23	SYN
6516.08	Fe II	2.89	-3.44	54.4	71.3	57.3	...	60.9	71.2	50.3	54.4	36.5	44.3	32	EW
5301.03	Co I	1.71	-1.94	33	SYN
5369.56	Co I	1.74	-1.59	33	SYN
5483.35	Co I	1.71	-1.41	33	SYN
5530.71	Co I	1.71	-2.23	57.7	...	47.2	33	EW
5590.64	Co I	2.04	-1.87	...	52.4	50.4	44.1	34	EW
5647.23	Co I	2.28	-1.56	...	41.4	41.4	51.9	34	EW
6770.97	Co I	1.88	-1.97	...	106.6	41.6	77.1	...	89.7	...	17.8	34	EW
6814.96	Co I	1.95	-1.90	...	92.7	49.2	69.7	83.6	34	EW
6872.44	Co I	2.01	-1.85	67.0	34	EW
7052.87	Co I	1.95	-1.62	...	116.1	63.8	94.6	95.8	127.4	...	22.6	34	EW
4953.16	Ni I	3.74	-0.58	82.3	35	EW
5003.73	Ni I	1.68	-2.80	107.1	67.0	125.3	23	EW
5084.10	Ni I	3.68	0.03	87.6	100.1	...	62.9	70.9	...	66.8	67.5	...	50.1	23	EW
5115.40	Ni I	3.83	-0.11	90.5	76.4	67.5	64.0	23	EW
5435.88	Ni I	1.99	-2.59	77.4	87.5	78.8	42.2	32.6	127.2	86.3	112.6	...	51.8	23	EW
5847.04	Ni I	1.68	-3.21	50.5	91.1	40.8	71.9	68.6	77.4	23	EW
6108.13	Ni I	1.68	-2.45	137.6	149.2	102.7	56.5	72.1	161.7	113.9	149.2	...	63.1	23	EW
6128.95	Ni I	1.68	-3.33	73.6	73.8	47.2	68.2	95.0	23	EW
6314.65	Ni I	1.94	-1.77	124.5	131.4	97.7	...	85.9	131.8	118.8	...	55.4	59.5	23	EW
6327.60	Ni I	1.68	-3.15	111.2	111.4	68.9	48.0	...	108.7	80.9	108.3	...	47.9	23	EW
6482.81	Ni I	1.94	-2.63	98.8	118.1	67.3	...	65.3	78.7	91.6	92.9	...	30.7	23	EW
6532.88	Ni I	1.94	-3.39	60.2	69.0	29.6	...	59.1	2	EW
6643.64	Ni I	1.68	-2.30	158.0	182.7	134.9	125.2	136.6	155.6	153.3	190.1	89.3	92.9	23	EW
6767.78	Ni I	1.83	-2.17	138.2	157.8	130.5	103.9	104.5	116.6	144.9	168.7	83.7	83.2	23	EW

Table 2—Continued

Wavelength Å	Species	E.P. eV	log gf	N1898 #1	N1898 #2	N2005 #1	N2005 #2	N2005 #3	N2019 #1	N2019 #2	N2019 #3	Hodge11 #1	Hodge11 #2	Source	EW or SYN
6772.30	Ni I	3.66	-0.98	57.7	57.6	29.6	53.7	43.8	42.5	23	EW
6914.56	Ni I	1.95	-1.47	155.3	...	107.7	86.9	78.9	152.2	160.2	165.6	...	68.1	23	EW
7062.98	Ni I	1.95	-3.50	38.8	49.5	34.7	57.5	23	EW
7110.91	Ni I	1.94	-2.97	87.3	101.7	48.4	...	39.3	98.9	72.5	74.4	23	EW
7122.21	Ni I	3.54	0.05	123.3	136.5	98.2	56.2	80.8	113.2	116.3	121.9	52.9	62.7	23	EW
7197.02	Ni I	1.94	-2.68	147.7	132.3	102.2	103.8	64.3	132.9	115.8	44.8	23	EW
5105.50	Cu I	1.39	-3.72	36	SYN
5782.05	Cu I	1.64	-2.92	36	SYN
4854.87	Y II	0.99	-0.38	90.7	37	SYN
4883.69	Y II	1.08	0.07	104.9	142.1	114.3	128.5	...	90.6	37	EW
5087.43	Y II	1.08	-0.17	72.4	85.4	70.3	95.9	78.0	...	58.5	72.6	...	56.0	37	SYN
5200.42	Y II	0.99	-0.57	84.8	68.1	61.1	...	50.7	101.3	85.3	56.0	55.1	55.8	37	SYN
5509.91	Y II	0.99	-1.01	59.0	60.6	45.8	59.2	61.2	59.6	37	SYN
5311.46	Zr I	0.52	-1.71	4	EW
6127.48	Zr I	0.15	-1.06	36.9	49.5	38.0	58.1	7	SYN
6134.57	Zr I	0.00	-1.28	31.8	53.2	36.2	53.8	82.9	7	EW
6143.18	Zr I	0.07	-1.10	28.8	68.8	39.7	52.0	91.2	7	EW
5853.69	Ba II	0.60	-1.02	139.6	181.6	127.6	107.4	...	154.7	137.2	167.7	104.0	102.6	38	EW
6496.90	Ba II	0.60	-0.37	217.9	244.6	194.2	170.3	168.2	196.0	182.8	221.1	142.5	144.2	38	EW
5114.51	La II	0.24	-1.03	77.6	66.6	60.3	89.9	73.7	102.6	39	EW
5301.86	La II	0.40	-1.14	39	SYN
6390.47	La II	0.32	-1.41	41.1	46.9	39.1	...	50.2	39	EW
6774.33	La II	0.13	-1.71	35.2	62.3	44.9	47.1	39	EW
4959.19	Nd II	0.06	-0.80	104.5	140.5	68.5	...	48.0	92.9	40	SYN
5092.80	Nd II	0.38	-0.61	72.3	64.5	98.2	40	EW
5212.35	Nd II	0.20	-0.96	80.7	106.9	95.1	84.0	137.8	40	EW
5234.21	Nd II	0.55	-0.51	80.7	63.7	76.4	62.8	66.4	40	SYN
5249.58	Nd II	0.98	0.20	...	93.8	46.9	77.2	71.4	89.4	40	EW
5255.52	Nd II	0.20	-0.67	91.6	94.3	37.9	94.9	79.4	92.3	40	SYN
5293.18	Nd II	0.82	0.10	87.8	122.3	37.4	94.1	101.9	119.4	40	EW
6645.13	Eu II	1.38	0.12	36.6	42.3	23.4	60.1	54.7	77.4	71.0	...	41	EW

References. — 1. M5-I01; 2. Shetrone et al. 2001; 3. Garz 1973; 4. Kurucz & Bell 1995; 5. Smith & Raggett 1981; 6. McWilliam et al. 1995; Ramírez & Cohen 2003; 8. Lawler & Dakin 1989; 9. Blackwell et al. 1983^a; 10. Martin, Fuhr, & Wiese 1988, 11. Nitz, Wickliffe, & Lawler 1998; 12. Blackwell et al. 1986^a; 13. Blackwell et al. 1982a^a

; 14. Blackwell et al. 1982b^a ; 15. Pickering, Thorne, & Perez 2001; 16. Whaling et al. 1985; 17. Tozzi, Brunner, & Huber 1985; 18. Blackwell et al. 1984; 19. Booth, Shallis, & Wells 1983; 20. O'Brian et al. 1991; 21. May, Richter, & Wichelmann 1974; 22. Bard, Kock, & Kock 1991; 23. Fuhr, Martin, & Wiese 1988; 24. Blackwell, Petford, & Shallis 1979; 25. Blackwell et al. 1979; 26. Blackwell et al. 1982c; 27. Bard & Kock 1994; 28. Blackwell et al. 1980; 29. Blackwell, Petford, & Simmons 1982; 30. Kroll & Kock 1987; 31. Schnabel, Kock, & Holweger 1999; 32. Heise & Kock 1990; 33. Nitz et al. 1999; 34. Cardon et al. 1982; 35. Wickliffe & Lawler 1997; 36. Simmerer et al. (2004); 37. Hannaford et al. 1982; 38. Kastberg et al. 1993; 39. Lawler, Bonvallet, & Sneden 2001; 40. Den Hartog et al. 2003 41. Lawler et al. 2001

^aRenormalized as suggested by Grevesse, Blackwell, & Petford (1989)

Table 3. Hyperfine Structure Information

$\lambda(\text{\AA})$	log gf
Sc II (E.P. = 1.77 eV, log gf = +0.02)	
5526.800	-2.775
5526.804	-2.372
5526.809	-1.562
5526.809	-2.160
5526.812	-1.357
5526.812	-2.050
5526.815	-1.291
5526.816	-2.029
5526.818	-1.295
5526.819	-0.633
5526.819	-2.138
5526.820	-1.356
5526.821	-0.754
5526.822	-1.478
5526.822	-1.661
5526.823	-0.890
5526.824	-1.046
5526.825	-1.231
5526.825	-1.807
5526.825	-1.465
Sc II (E.P. = 1.50 eV, log gf = -1.13)	
5640.98	-1.654
5640.98	-2.143
5640.99	-1.946
5640.99	-2.841
5640.99	-2.027
5641.00	-2.404
5641.00	-2.404

Table 3—Continued

$\lambda(\text{\AA})$	log gf
5641.00	-2.146
5641.00	-2.132
Sc II (E.P. = 1.51 eV, log gf = -0.60)	
5657.870	-1.226
5657.871	-1.796
5657.876	-1.796
5657.878	-1.624
5657.879	-1.638
5657.883	-1.638
5657.884	-2.320
5657.886	-1.649
5657.888	-1.649
5657.889	-3.746
5657.890	-1.822
5657.892	-1.822
5657.893	-1.998
Sc II (E.P. = 1.50 eV, log gf = -1.36)	
5667.137	-1.954
5667.143	-2.150
5667.148	-2.150
5667.153	-3.335
5667.157	-2.154
5667.162	-2.154
5667.166	-2.409
Sc II (E.P. = 1.5 eV, log gf = -1.07)	
6245.604	-1.672
6245.613	-2.412

Table 3—Continued

$\lambda(\text{\AA})$	log gf
6245.614	-1.843
6245.620	-3.412
6245.622	-2.229
6245.623	-2.050
6245.627	-2.994
6245.629	-2.196
6245.630	-2.321
6245.633	-2.760
6245.635	-2.255
6245.636	-2.739
6245.638	-2.614
6245.639	-2.438
6245.641	-2.517
Sc II (E.P. = 1.36 eV, log gf = -1.31)	
6604.581	-2.506
6604.589	-2.348
6604.593	-1.936
6604.595	-2.359
6604.599	-2.334
6604.601	-2.532
6604.603	-3.030
6604.606	-4.456
6604.609	-2.708
6604.610	-2.506
6604.612	-2.348
6604.614	-2.359
6604.614	-2.532
V I (E.P. = 0.00 eV, log gf = -1.14)	
4851.467	-1.946

Table 3—Continued

$\lambda(\text{\AA})$	log gf
4851.480	-1.925
4851.486	-2.402
4851.498	-2.071
4851.504	-1.925
4851.526	-1.604
V I (E.P. = 1.06 eV, log gf = -0.65)	
6039.727	-1.854
6039.729	-1.854
6039.730	-2.030
6039.733	-1.690
6039.733	-2.155
6039.734	-2.280
6039.738	-1.682
6039.738	-1.716
6039.739	-2.708
6039.744	-1.843
6039.744	-1.433
6039.751	-1.217
V I (E.P. = 1.05 eV, log gf = -0.58)	
6081.426	-1.608
6081.426	-1.784
6081.436	-1.608
6081.437	-1.483
6081.451	-1.483
6081.451	-1.597
6081.451	-1.802
6081.469	-1.597
6081.469	-1.186

Table 3—Continued

$\lambda(\text{\AA})$	log gf
V I (E.P. = 1.08 eV, log gf = -0.06)	
6090.206	-0.690
6090.213	-0.831
6090.219	-0.995
6090.219	-1.530
6090.225	-1.334
6090.225	-1.193
6090.229	-1.280
6090.229	-1.448
6090.231	-2.644
6090.232	-1.302
6090.233	-1.836
6090.235	-2.234
6090.235	-1.393
6090.237	-2.012
6090.238	-1.581
6090.239	-1.887
6090.240	-1.836
6090.240	-1.866
V I (E.P. = 1.04 eV, log gf = -0.72)	
6111.592	-1.681
6111.632	-1.204
6111.656	-1.204
6111.695	-1.350
V I (E.P. = 1.06 eV, log gf = -0.32)	
6119.495	-1.348
6119.495	-1.524
6119.506	-1.348

Table 3—Continued

$\lambda(\text{\AA})$	log gf
6119.506	-1.223
6119.520	-1.223
6119.521	-1.542
6119.521	-1.337
6119.539	-1.337
6119.539	-0.926
V I (E.P. = 1.05 eV, log gf = -0.75)	
6135.347	-1.535
6135.347	-1.556
6135.347	-1.681
6135.387	-2.012
6135.387	-1.535
6135.388	-1.214
V I (E.P. = 0.0 eV, 3 log gf = -1.78)	
6150.170	-2.484
6150.186	-2.568
6150.200	-2.658
6150.212	-2.754
6150.225	-2.858
6150.227	-3.631
6150.235	-3.413
6150.235	-2.970
6150.243	-3.331
6150.245	-3.088
6150.250	-3.315
6150.253	-3.206
6150.256	-3.351
6150.260	-3.447
6150.264	-3.658

Table 3—Continued

$\lambda(\text{\AA})$	log gf
6150.277	-5.084
6150.279	-4.658
6150.279	-4.695
6150.281	-4.503
6150.281	-4.451
6150.281	-4.423
V I (E.P. = 0.29 eV, log gf = -1.30)	
6199.138	-1.973
6199.155	-2.078
6199.171	-2.194
6199.186	-2.323
6199.190	-2.981
6199.198	-2.469
6199.201	-2.770
6199.209	-2.639
6199.210	-2.697
6199.218	-2.691
6199.219	-2.843
6199.224	-2.738
6199.227	-3.106
6199.229	-2.843
6199.231	-3.039
6199.235	-4.282
6199.240	-3.884
6199.242	-3.738
6199.243	-3.680
6199.243	-3.583
6199.244	-3.583
V I (E.P. = 0.28 eV, log gf = -1.29)	

Table 3—Continued

$\lambda(\text{\AA})$	log gf
6216.432	-1.920
6216.449	-2.061
6216.465	-2.225
6216.478	-2.760
6216.479	-2.423
6216.489	-2.564
6216.491	-2.678
6216.498	-2.510
6216.501	-3.066
6216.505	-2.532
6216.510	-2.623
6216.514	-2.811
6216.518	-3.874
6216.521	-3.096
6216.522	-3.464
6216.523	-3.066
6216.524	-3.242
6216.525	-3.117
V I (E.P. = 0.29 eV, log gf = -2.01)	
6224.466	-3.594
6224.477	-3.390
6224.485	-3.325
6224.494	-3.332
6224.501	-2.691
6224.502	-3.398
6224.506	-2.878
6224.508	-3.536
6224.510	-3.097
6224.514	-3.360
6224.515	-3.816
6224.517	-3.691

Table 3—Continued

$\lambda(\text{\AA})$	log gf
6224.519	-4.138
6224.520	-4.837
6224.525	-3.816
6224.530	-3.536
6224.534	-3.398
6224.536	-3.332
6224.539	-3.325
6224.540	-3.390
6224.541	-3.594
V I (E.P. = 0.28 eV, log gf = -2.07)	
6233.169	-3.415
6233.175	-3.234
6233.181	-3.203
6233.187	-3.267
6233.192	-3.466
6233.198	-2.716
6233.200	-3.008
6233.201	-3.414
6233.202	-4.131
6233.202	-5.374
6233.203	-3.721
6233.212	-3.466
6233.217	-3.267
6233.221	-3.203
6233.225	-3.234
6233.229	-3.415
V I (E.P. = 0.29 eV, log gf = -1.34)	
6251.764	-2.924
6251.781	-2.720

Table 3—Continued

$\lambda(\text{\AA})$	log gf
6251.796	-2.655
6251.799	-2.021
6251.810	-2.662
6251.811	-2.208
6251.821	-2.427
6251.822	-2.728
6251.830	-2.690
6251.832	-2.866
6251.837	-3.021
6251.840	-3.146
6251.842	-3.468
6251.845	-4.167
6251.846	-2.924
6251.851	-2.720
6251.852	-3.146
6251.855	-2.655
6251.855	-2.866
6251.857	-2.662
6251.857	-2.728
V I (E.P. = 0.27 eV, log gf = -1.67)	
6274.639	-2.932
6274.660	-2.455
6274.672	-2.476
6274.687	-2.134
6274.688	-2.455
6274.709	-2.601
V I (E.P. = 0.28 eV, log gf = -1.51)	
6285.108	-3.568
6285.127	-3.140

Table 3—Continued

$\lambda(\text{\AA})$	log gf
6285.132	-2.703
6285.144	-2.890
6285.147	-2.542
6285.158	-2.714
6285.158	-2.550
6285.162	-2.077
6285.167	-2.714
6285.171	-2.293
6285.178	-2.576
6285.182	-3.015
Mn I (E.P. = 0.00 eV, log gf = -3.50)	
5394.669	-4.067
5394.702	-4.985
5394.705	-4.207
5394.728	-6.202
5394.731	-4.809
5394.734	-4.365
5394.752	-5.850
5394.755	-4.783
5394.757	-4.549
5394.771	-5.725
5394.773	-4.850
5394.775	-4.771
5394.784	-5.804
5394.786	-5.026
5394.786	-5.056
Mn I (E.P. = 2.14 eV, log gf = -1.46)	
5420.273	-3.016
5420.278	-2.986

Table 3—Continued

$\lambda(\text{\AA})$	log gf
5420.288	-2.731
5420.289	-3.764
5420.298	-2.810
5420.312	-2.509
5420.314	-3.685
5420.327	-2.743
5420.346	-2.325
5420.349	-3.810
5420.366	-2.769
5420.389	-2.167
5420.394	-4.162
5420.416	-2.945
5420.443	-2.027
Mn I (E.P. = 0.00 eV, log gf = -3.80)	
5432.530	-4.382
5432.534	-5.160
5432.559	-5.160
5432.562	-4.645
5432.565	-4.997
5432.584	-4.997
5432.587	-4.976
5432.589	-4.992
5432.604	-4.992
5432.606	-5.423
5432.607	-5.094
5432.617	-5.094
5432.619	-6.122
5432.620	-5.356
5432.625	-5.356
Mn I (E.P. = 2.18 eV, log gf = -1.85)	

Table 3—Continued

$\lambda(\text{\AA})$	log gf
5516.693	-3.276
5516.703	-2.908
5516.713	-2.908
5516.722	-4.485
5516.737	-2.776
5516.752	-2.776
5516.767	-2.950
5516.786	-2.878
5516.806	-2.878
5516.825	-2.401
Mn I (E.P. = 3.07 eV, log gf = -0.25)	
6013.520	-0.765
6013.545	-0.977
6013.567	-1.250
6013.573	-1.454
6013.584	-1.660
6013.587	-1.308
6013.598	-1.329
6013.605	-1.484
6013.615	-2.408
6013.615	-1.806
6013.619	-2.028
6013.619	-1.852
Mn I (E.P. = 3.07 eV, log gf = +0.03)	
6021.712	-2.672
6021.738	-1.455
6021.744	-2.320
6021.766	-1.279

Table 3—Continued

$\lambda(\text{\AA})$	log gf
6021.770	-0.537
6021.771	-2.195
6021.787	-1.253
6021.791	-0.677
6021.792	-2.274
6021.802	-1.320
6021.807	-0.835
6021.813	-1.496
6021.818	-1.019
6021.823	-1.241
6021.823	-1.526
Co I (E.P. = 1.71 eV, log gf = -1.94)	
5301.059	-3.285
5301.059	-2.586
5301.060	-2.878
5301.060	-3.104
5301.060	-3.073
5301.061	-3.285
5301.061	-3.104
5301.061	-3.284
5301.061	-3.137
5301.061	-3.073
5301.061	-4.001
5301.061	-3.137
5301.061	-5.244
5301.061	-3.336
5301.061	-3.336
5301.061	-3.591
Co I (E.P. = 1.74 eV, log gf = -1.59)	

Table 3—Continued

$\lambda(\text{\AA})$	log gf
5369.579	-2.157
5369.580	-2.373
5369.580	-2.656
5369.580	-2.783
5369.580	-2.622
5369.580	-2.630
5369.580	-3.095
5369.581	-3.648
5369.581	-3.220
5369.581	-2.970
5369.581	-2.794
5369.581	-2.794
Co I (E.P. = 1.71 eV, log gf = -1.41)	
5483.389	-2.040
5483.390	-2.880
5483.390	-2.181
5483.390	-2.684
5483.390	-2.345
5483.391	-3.994
5483.391	-2.630
5483.391	-2.543
5483.391	-2.798
5483.392	-3.584
5483.392	-3.362
5483.392	-2.652
5483.392	-2.743
5483.392	-3.186
5483.392	-2.931
5483.392	-3.237
5483.392	-3.186
5483.392	-3.216

Table 3—Continued

$\lambda(\text{\AA})$	log gf
Co I (E.P. = 1.71 eV, log gf = -2.23)	
5530.789	-2.860
5530.790	-3.001
5530.790	-3.700
5530.790	-3.165
5530.791	-4.814
5530.791	-3.504
5530.791	-3.450
5530.791	-3.363
5530.791	-4.404
5530.791	-4.182
5530.791	-3.472
5530.791	-3.618
5530.791	-3.563
5530.791	-4.006
5530.792	-4.057
5530.792	-4.006
5530.792	-3.751
5530.792	-4.036
Co I (E.P. = 2.04 eV, log gf = -1.87)	
5590.708	-2.887
5590.708	-2.476
5590.710	-3.092
5590.710	-2.773
5590.710	-2.887
5590.711	-2.898
5590.712	-2.773
5590.712	-3.074
5590.713	-2.898

Table 3—Continued

$\lambda(\text{\AA})$	log gf
Co I (E.P. = 2.28 eV, log gf = -2.13)	
5647.229	-2.127
5647.230	-2.343
5647.230	-2.626
5647.230	-2.753
5647.230	-2.592
5647.230	-2.600
5647.230	-3.065
5647.231	-3.618
5647.231	-3.190
5647.231	-2.940
5647.231	-2.764
5647.231	-2.764
Co I (E.P. = 1.88 eV, log gf = -1.97)	
6770.972	-3.011
6770.972	-3.011
6770.972	-3.011
6770.973	-3.011
6770.973	-3.011
6770.974	-3.011
6770.974	-3.011
6770.975	-3.011
6770.975	-3.011
6770.976	-3.011
6770.977	-3.011
Co I (E.P. = 1.95 eV, log gf = -1.90)	
6814.958	-2.917

Table 3—Continued

$\lambda(\text{\AA})$	log gf
6814.959	-2.506
6814.959	-2.803
6814.960	-2.928
6814.960	-3.122
6814.961	-3.104
6814.961	-2.917
6814.962	-2.803
6814.962	-2.928
Co I (E.P. = 2.01 eV, log gf = -1.85)	
6872.438	-2.334
6872.439	-2.811
6872.441	-2.480
6872.443	-2.334
Co I (E.P. = 1.95 eV, log gf = -1.62)	
7052.868	-2.187
7052.869	-2.403
7052.870	-2.686
7052.871	-2.813
7052.871	-2.652
7052.871	-3.125
7052.872	-2.660
7052.872	-2.824
7052.873	-3.678
7052.873	-3.250
7052.873	-3.000
7052.873	-2.824

References. — Sc: Mansour et al. 1989; V: Childs et al. 1979; Palmeri et al. 1995; Cochrane et al. 1998 and references therein; Mn: Lefébvre, Garnir, & Biémont 2003 and references therein; Co: Pickering 1996 and references therein.